J. Fluid Mech. (1995), *vol.* 288, *pp.* 201–248

Simplified equations for the interaction of nearly parallel vortex filaments

By RUPERT KLEIN[1], ANDREW J. MAJDA[2] AND KUMARAN DAMODARAN[3]

[1] Institut fur Technische Mechanik, RWTH, Templergraben 64, 52056, Aachen, Germany

[2] Department of Mathematics and Program in Applied and Computational Mathematics, Princeton University, Princeton, NJ 08544, USA

[3] Department of Applied Mathematics and Theoretical Physics, University of Cambridge, Silver Street, Cambridge CB3 9EW, UK

(Received 22 August 1994 and in revised form 8 November 1994)

New simplified asymptotic equations for the interaction of nearly parallel vortex filaments are derived and analysed here. The simplified equations retain the important physical effects of linearized local self-induction and nonlinear potential vortex interaction among different vortices but neglect other non-local effects of self-stretching and mutual induction. These equations are derived systematically in a suitable distinguished asymptotic limit from the Navier–Stokes equations. The general Hamiltonian formalism and conserved quantities for the simplified equations are developed here. Properties of these asymptotic equations for the important special case involving nearly parallel pairs of interacting filaments are developed in detail. In particular, strong evidence is presented that for any filament pair with a negative circulation ratio, there is finite-time collapse in a self-similar fashion independent of the perturbation but with a structure depending on the circulation ratio. On the other hand, strong evidence is presented that no finite-time collapse is possible for perturbations of a filament pair with a positive circulation ratio. The present theory is also compared and contrasted with earlier linear and nonlinear stability analyses for pairs of filaments.

1. Introduction

Nearly parallel interacting vortex filaments with large strength and narrow cross-section are prominent fluid mechanical structures in mixing layers (Corcos & Lin 1984), boundary layers, and trailing wakes (Van Dyke 1982). Contemporary turbulence theories for structure in the inertial range (Chorin 1988; Chorin & Akao 1991) also emphasize the dynamics of slender vortex filaments. Thus, it is very interesting to develop simplified asymptotic equations for the interaction of nearly parallel vortex filaments in high-Reynolds-number flows.

The main purpose of the work presented here is to derive a new simplified system of asymptotic equations for the interaction of an arbitrary number of nearly parallel vortex filaments in a suitable distinguished asymptotic limit (see §§2 and 3); the properties of solutions of these new equations are analysed in detail in §§4 and 5 for the special case of a pair of interacting nearly parallel vortex filaments. Also, in §6 of this paper the new asymptotic equations are compared with linear theories (Crow 1970); Moore & Saffman 1972; Widnall 1975) as well as a recent nonlinear theory (Klein & Majda 1993) for nearly parallel interacting filament pairs; it is established that

the equations in the present work are the appropriate dynamical equations describing the nonlinear evolution of the long-wave linear vortex pair instabilities found in the earlier studies. The work presented here is an outgrowth of the authors' attempt to understand a very interesting remark of Zakharov (1988) regarding symmetric perturbations of anti-parallel vortex pairs and in §4, we derive a variant of the equation of Zakharov as an extreme special case of our general theory.

The asymptotic equations which we derive and analyse in this paper are the following: consider N-vortex filaments which are all nearly parallel to the z-axis with their perturbed centrelines described by the pairs of coordinates

$$\boldsymbol{X}_j(\sigma, t) = (x_j(\sigma, t), y_j(\sigma, t)) \quad (1 \leqslant j \leqslant N), \tag{1.1}$$

where σ parameterizes the z-axis and $\sigma, t, \boldsymbol{X}_j$ are suitably scaled variables in an appropriate asymptotic development (see §2). Then the self-consistent simplified asymptotic limiting equations for N-nearly parallel interacting vortex filaments derived in §2 have the form

$$\frac{\partial \boldsymbol{X}_j}{\partial t} = J\left[\alpha_j \Gamma_j \frac{\partial^2}{\partial \sigma^2} \boldsymbol{X}_j\right] + J\left[\sum_{k \neq j}^{N} 2\Gamma_k \frac{(\boldsymbol{X}_j - \boldsymbol{X}_k)}{|\boldsymbol{X}_j - \boldsymbol{X}_k|^2}\right] \quad (1 \leqslant j \leqslant N), \tag{1.2}$$

where J is the skew-symmetric matrix

$$J = \begin{pmatrix} 0 & -1 \\ 1 & 0 \end{pmatrix}. \tag{1.3}$$

The quantity Γ_j in (1.2) is the circulation of the jth vortex and α_j is a constant determined by the vortex core structure through an asymptotic matching procedure (Callegari & Ting 1978; Ting & Klein 1991; Klein & Majda 1991*a*; Klein & Knio 1994).

1.1. *Heuristic derivation of the asymptotic equations*

It is interesting to give a heuristic explanation of the equations in (1.2) without any asymptotic formalism. If we ignore the first term on the right-hand side of (1.2), the equations that result

$$\frac{\partial \boldsymbol{X}_j}{\partial t} = J\left[\sum_{k \neq j}^{N} 2\Gamma_k \frac{(\boldsymbol{X}_j - \boldsymbol{X}_k)}{|\boldsymbol{X}_j - \boldsymbol{X}_k|^2}\right], \tag{1.4}$$

are the familiar equations for the interaction of two-dimensional point-vortices where every vortex moves in the potential field generated by the other vortices (Lamb 1932); here these equations act in a layered fashion for every value of σ. In particular, general solutions of the equations for point vortex motion in two dimensions (Aref 1983) are always special σ-independent exact solutions of (1.2). In §3, we generalize the well-known Hamiltonian structure and conserved quantities for (1.4) to the general equations in (1.2).

On the other hand, the simplest asymptotic equation for the motion of a single vortex filament is the local self-induction equation derived by Hama and Arms (Batchelor 1967)

$$\frac{\partial \boldsymbol{X}}{\partial t} = C_0 \boldsymbol{t} \times \frac{\partial^2}{\partial \sigma^2} \boldsymbol{X}, \tag{1.5}$$

where C_0 is a constant related to the choice of reference time and $\boldsymbol{t}$ is the unit tangent

vector. The local self-induction equation linearized about a filament parallel to the z-axis and evaluated for the perturbed filament $\boldsymbol{X}_j$ is given by

$$\frac{\partial \boldsymbol{X}_j}{\partial t} = J\left[\alpha_j \Gamma_j \frac{\partial^2}{\partial \sigma^2} \boldsymbol{X}_j\right], \tag{1.6}$$

where, for convenience, we have used the choice of the constant C_0 determined by $\alpha_j \Gamma_j$ for the jth vortex through the matching procedure in §2. Looking back at (1.2), we observe that the first term on the right-hand side involves the physical effect of self-induction linearized about the straight background filament. In particular, more complex effects of self-stretching of vortex filaments (Klein & Majda 1991*a*, *b*) as discussed in §6 of this paper are ignored in the asymptotic equations in (1.2).

To summarize the discussion in the last two paragraphs, we see that the asymptotic equations in (1.2) merely involve the sum of two different but important physical effects for interacting nearly parallel vortex filaments, the linearized self-induction of each individual vortex line and the nonlinear potential vortex interaction of the other vortices acting on an individual vortex in a layered fashion. Intuition suggests that these two physical effects might dominate for nearby interacting almost parallel vortex filaments where the wavelength of the perturbations is much longer than the separation distance and this separation distance is much larger than the core thickness. This intuition is confirmed by the detailed asymptotic derivation for (1.2) summarized in §2. On the other hand, the recent nonlinear theory of Klein & Majda (1993) for anti-parallel vortex filaments applies for smaller perturbation amplitudes in a different regime where the wavelength is comparable to the separation distance and consequently other more complex effects of non-local self-stretching and mutual induction also contribute in a non-trivial fashion. A detailed comparison and discussion of these two distinct asymptotic regimes is presented in §6 of this paper.

1.2. *Interacting pairs of nearly parallel vortex filaments*

The solutions of the equations in (1.2) are studied in §§4 and 5 for pairs of interacting filaments with a circulation ratio Γ which can always be normalized to satisfy $-1 \leqslant \Gamma \leqslant 1, \Gamma \neq 0$; we also assume the same vortex core structure so that $\alpha_j = 1$ in (1.2) for $j = 1, 2$. The anti-parallel vortex pair has the value $\Gamma = -1$ and the co-rotating vortex pair has the value $\Gamma = 1$. In §4 we develop a linearized stability analysis with the result that within the asymptotic equations in (1.2), vortex pairs are linearly unstable with a long wavelength band of instability for Γ with $-1 \leqslant \Gamma < 0$ and vortex pairs are linearly (neutrally) stable for Γ with $0 < \Gamma \leqslant 1$. We also find special exact nonlinear solutions for the equations in (1.2) with $\Gamma = 1$ and easily recover essentially Zakharov's equations (Zakharov 1988) for the special case of symmetric perturbations and $\Gamma = -1$.

We study the nonlinear behaviour of the nearly parallel filament pair within the asymptotic approximation in (1.2) through numerical calculations in §5. We give very strong numerical evidence for robust finite-time collapse of a pair of perturbed interacting vortex filaments for any negative circulation ratio, Γ, with $-1 \leqslant \Gamma < 0$; furthermore, the finite-time collapse has an asymptotically self-similar form which depends on the circulation ratio, Γ, but is universal and completely independent of the nature of the perturbation for a fixed circulation ratio. On the other hand, for any positive circulation ratio, Γ, with $0 < \Gamma \leqslant 1$, we present strong numerical evidence that no finite-time collapse is possible for a wide variety of general large-amplitude perturbations of the vortex configuration. The notion of finite-time collapse means that the two filament curves actually touch in a finite time during the temporal evolution

under (1.2). Of course, solutions of the asymptotic equations in (1.2) are no longer valid as a physical approximation when the separation distance is comparable to the asymptotic core size (see §2); nevertheless, it is interesting that linearized self-induction and the nonlinear potential vortex interaction in (1.2) are the only physical effects needed to drive two filaments with negative circulation ratios very close together. At distances where the core thickness and separation distance are comparable, many recent numerical experiments give strong evidence for substantial core flattening and vortex reconnection (Anderson & Greengard 1989; Kerr & Hussain 1989; Meiron *et al.* 1989; Melander & Zabusky 1987; Kida & Takaoka 1991). Clearly the simplified asymptotic equations in (1.2) cannot account for any of these effects.

2. Derivation

Here we outline the key ideas and calculations that lead to the simplified equations for interacting vortex filaments in (1.2). An ensemble of N vortex filaments, as sketched in figure 1, interacts via the three-dimensional Biot-Savart integrals for the induced velocities on the filament centrelines (see Klein & Knio (1994) for a detailed analysis). The integrals decompose into the sum of the Biot-Savart integrals over the vorticities of each individual vortex, so that the induced motion of one given filament consists of self- and foreign-induced velocity contributions. The self-induction of slender perturbed vortices in the regime considered in this paper has been studied in detail by Klein & Majda (1991*a*) and we will use their results here without repeating the derivation. Thus, in the present section and in the Appendix we concentrate on the velocity contributions due to the presence of the neighbouring filaments. A leading-order asymptotic derivation of the equations in (1.2), which is self-contained except for a few references to specialized differential geometric relations, is provided in the present section. Since non-local induction effects turned out to be very important in other regimes for slender vortex dynamics (Klein & Majda 1991*b*, 1993; Klein, Majda & McLaughlin 1992), we present in the Appendix a detailed calculation that includes higher-order terms and demonstrates that, in the regime considered in this paper, the curvature-potential vortex interaction proposed on intuitive grounds in §1 in fact arises as the leading-order dynamics from a systematic analysis under a suitable distinguished limit of perturbation wavelengths, perturbation amplitudes and vortex core sizes.

We consider N slender, nearly parallel vortex filaments that are characterized individually by

$$\left.\begin{aligned} &\text{(i) the circulation strengths, } \Gamma_i, \\ &\text{(ii) the small effective core sizes, } \delta_i \ll 1 \\ \text{and} \quad &\text{(iii) the time-dependent centrelines } \mathscr{L}_i^\epsilon(t). \end{aligned}\right\} \tag{2.1}$$

Following Klein & Majda (1991*a*), length and time are non-dimensionalized using a characteristic radius of curvature of the $\mathscr{L}_i^\epsilon$-curves and a typical circulation strength, so that all the Γ_i are of order $O(1)$. The core size parameters δ_i for the individual filaments are given by

$$\delta_i = \delta \exp(-C_i) \quad (\delta \ll 1), \tag{2.2}$$

where $C_i = O(1)$ is a quadratically nonlinear functional of the detailed core vorticity distribution of the ith filament (see Callegari & Ting 1978; Klein & Majda 1991*a*; Klein & Knio 1995). The centrelines $\mathscr{L}_i^\epsilon(t)\colon s \to \boldsymbol{X}_i^\epsilon(s,t)$ have an asymptotic representation

$$\boldsymbol{X}_i^\epsilon(s,t) = s\boldsymbol{t}_0 + \epsilon^2 \boldsymbol{X}_i^{(2)}\left(\frac{s}{\epsilon}, \frac{t}{\epsilon^4}\right) + o(\epsilon^2), \tag{2.3}$$

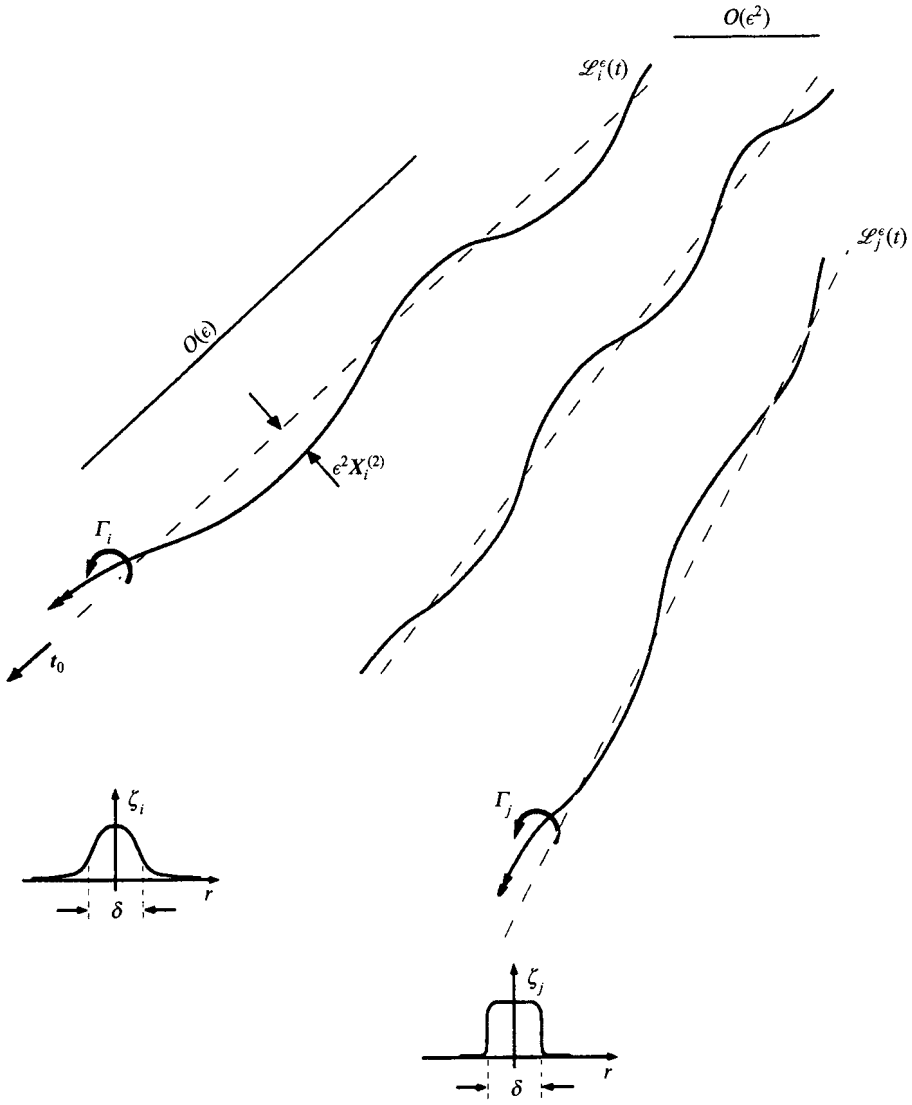

FIGURE 1. Vortex filaments characterized by circulation, Γ_i, core size δ, core vorticity distribution $\zeta_i(r/\delta)$ and filament centreline $\mathscr{L}_i^\epsilon(t)$.

where $\boldsymbol{t}_0$ is a constant unit vector and ϵ is a small parameter, satisfying

$$\delta \ll \epsilon^2 \ll 1. \tag{2.4}$$

Without loss of generality we require that the $\boldsymbol{X}_i^{(2)}$ are normal to $\boldsymbol{t}_0$, i.e. that $\boldsymbol{X}_i^{(2)} \cdot \boldsymbol{t}_0 \equiv 0$.

The formula in (2.3) represents small-amplitude, short-wavelength distortions of a leading-order straight vortex, while the order estimate in (2.4) accommodates displacements of the filaments that are in general large compared to the vortex core diameters. We introduce a particular distinguished limit between the core size parameter δ and the displacement parameter ϵ^2 in (2.12) below.

It has been shown by Callegari & Ting (1978), Klein & Majda (1991*a*) and, using a totally different analytical approach, by Klein (1994) and Klein & Knio (1995) that the

geometrical evolution of slender vortices in the regime considered obeys the propagation law

$$\frac{\partial \boldsymbol{X}_i}{\partial t} = \left(\ln\left(\frac{1}{\delta}\right) + C_i\right)\frac{\Gamma_i}{4\pi}(\kappa \boldsymbol{b})_i + \boldsymbol{Q}_i^f + \boldsymbol{Q}_i^{outer}. \tag{2.5}$$

The first term points in the direction of the local binormal vector $\boldsymbol{b}_i$ and, via the expression $(\ln(1/\delta)+C_i)$, describes the influence of the vortex core structure on the filament motion. The logarithmic term represents the overall effect of the core size, whereas the core coefficient C_i depends on the detailed core vorticity distribution as mentioned above. The contribution $\boldsymbol{Q}_i^f$ in (2.5) is the so-called finite part of the Bio-Savart integral and it describes the filament motion due to non-local self-induction. Finally, $\boldsymbol{Q}_i^{outer}$ is a superimposed velocity contribution, which in the present analysis corresponds to the induced velocity at the centreline location of the ith filament owing to the vorticities of the other filaments with $j = 1, \ldots, N, j \neq i$.

The local and non-local self-induction for a single filament with geometrical scalings as in (2.3) has been analysed in detail by Klein & Majda (1991*a*). The authors find, in particular, that $\boldsymbol{Q}_i^f$, which generally is a complex non-local and nonlinear functional of the filament geometry $\mathscr{L}_i(t)$, reduces under the stated assumptions to the linearized, yet still non-local, expression

$$\boldsymbol{Q}_i^{f,\epsilon} = \frac{\Gamma_i}{4\pi}\mathscr{I}[\boldsymbol{X}_i^{(2)}] \times \boldsymbol{t}_0 + o(1) \quad \text{as } \epsilon \to 0. \tag{2.6}$$

Here $\mathscr{I}[\cdot]$ is the pseudo-differential operator

$$\mathscr{I}[w](\sigma) = \int_{-\infty}^{\infty} \frac{1}{|h|^3}(w(\sigma+h) - w(\sigma) - hw'(\sigma+h) + \tfrac{1}{2}h^2 H(1-|h|)\, w''(\sigma))\, \mathrm{d}h, \tag{2.7}$$

where primes denote differentiation with respect to σ and $H(\cdot)$ is the Heaviside step. The impact of the $\mathscr{I}$-operator is best understood by considering its Fourier symbol

$$\hat{I}(\xi) = \mathrm{e}^{-\mathrm{i}\xi\sigma}\mathscr{I}[\mathrm{e}^{\mathrm{i}\xi\sigma}] = -\xi^2(\ln|\xi| - C_0), \tag{2.8}$$

where $C_0 = -0.0772\ldots$ is a given fixed constant, (see Klein & Majda 1991*a*).

Given these results for the self-induction of each filament, we are left with the task of analysing the foreign-induced velocity components $\boldsymbol{Q}_i^{outer}$. We show in the Appendix that this velocity contribution evaluates to the sum of the line-Biot-Savart integrals extended over all of the neighbouring filaments, i.e.

$$\boldsymbol{Q}_i^{outer}(\boldsymbol{X}_i, t) = -\sum_{\substack{j=1 \\ j \neq i}}^{N} \frac{\Gamma_j}{4\pi}\int_{\mathscr{L}_j^{\epsilon}(t)} \frac{\boldsymbol{X}_i - \boldsymbol{X}_j}{|\boldsymbol{X}_i - \boldsymbol{X}_j|^3} \times \mathrm{d}\boldsymbol{X}_j = \sum_{j \neq i} \boldsymbol{Q}_{j/i}^{outer}. \tag{2.9}$$

This formula provides an accurate approximation as long as $|\boldsymbol{X}_i - \boldsymbol{X}_j| \gg \delta$ everywhere, i.e. as long as there is no local merging between pairs of filaments.

Each of the integrals $\boldsymbol{Q}_{j/i}^{outer}$ under the sum in (2.9) is to be evaluated asymptotically using the curve representations in (2.3) for $\epsilon \ll 1$. Noticing that the reference point $\boldsymbol{X}_i$ on the ith filament is located far outside the core of, say, the jth filament, we may immediately use the explicit formulas given, e.g. by Callegari & Ting (1978) or Klein & Majda (1991*a*) for the induced velocity from a slender vortex in the immediate vicinity, but still outside, of its vortical core:

$$\boldsymbol{Q}_{j/i}^{outer} = \frac{\Gamma_j}{2\pi r_{j/i}}\boldsymbol{\theta}_{j/i} + \frac{\Gamma_j}{4\pi}\left\{\ln\left(\frac{1}{r_{j/i}}\right)(\kappa \boldsymbol{b})_{j/i} + (\kappa \cos\varphi \boldsymbol{\theta})_{j/i} + \boldsymbol{Q}_{j/i}^f\right\}. \tag{2.10}$$

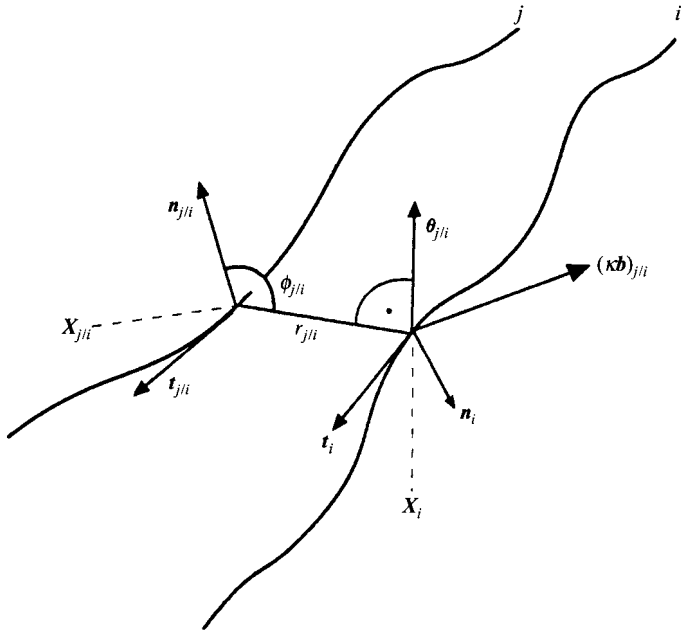

FIGURE 2. Associated points on neighbouring filaments and auxiliary quantities for the description of vortex–vortex interactions.

Here $r_{j/i}$ is the shortest distance between $\boldsymbol{X}_i$ and any point on $\mathscr{L}_j^\epsilon(t)$. Let the associated point on $\mathscr{L}_j^\epsilon$ closest to $\boldsymbol{X}_i$ be denoted by $\boldsymbol{X}_{j/i}$. Then $\boldsymbol{\theta}_{j/i}$ is the circumferential unit vector in planes normal to $\mathscr{L}_j^\epsilon$ in $\boldsymbol{X}_{j/i}$ evaluated at $\boldsymbol{X}_i$. Furthermore, $(\kappa \boldsymbol{b})_{j/i}$ is the product of curvature and binormal of $\mathscr{L}_j^\epsilon$ in $\boldsymbol{X}_{j/i}$ while $\varphi_{j/i}$ is the circumferential angle in the normal plane at $\boldsymbol{X}_{j/i}$, measured with respect to the principal normal $\boldsymbol{n}_{j/i}$. Finally $\boldsymbol{Q}_{j/i}^f$ is the finite part of the Biot-Savart-integral for $\mathscr{L}_j^\epsilon$, evaluated at $\boldsymbol{X}_{j/i}$. We illustrate the definitions of the symbols $(r, \varphi, \boldsymbol{\theta}, \boldsymbol{b})_{j/i}$ in figure 2. Next we obtain the leading-order contribution to (2.10) by observing that the distances $r_{j/i}$, following the curve representation in (2.3), are

$$r_{j/i} = \epsilon^2 |\boldsymbol{X}_{j/i}^{(2)} - \boldsymbol{X}_i^{(2)}|, \tag{2.11}$$

(see (A 12) in the Appendix), so that the first term in (2.10) is $O(\epsilon^{-2})$, while the other terms are $O(\ln 1/\epsilon)$ and $O(1)$ only. Considering on the other hand the equation of motion (2.5) for the ith filament, we find that the leading binormal term from the self-induction is of order $O(\ln 1/\delta)$. Obviously we obtain a highly non-trivial competition between local induction effects and the leading 'potential vortex term' in (2.10) if we introduce the distinguished limit

$$\epsilon^2 = \frac{1}{\ln 1/\delta}. \tag{2.12}$$

Under this constraint, we find the following preliminary set of evolution equations for the ensemble of filaments:

$$\frac{\partial \boldsymbol{X}_i}{\partial t} = \frac{1}{4\pi\epsilon^2}\left\{\alpha_i \Gamma_i (\kappa \boldsymbol{b})_i + \sum_{j \neq i} \frac{2\Gamma_j}{|\boldsymbol{X}_j^{(2)} - \boldsymbol{X}_i^{(2)}|}\boldsymbol{\theta}_{j/i}\right\}, \tag{2.13}$$

where

$$\alpha_i = \epsilon^2\left(\ln\frac{1}{\delta} + C_i\right) \tag{2.14}$$

characterizes the influence of the core structure of the ith filament. To obtain a closed system from these equations, we have to express the time derivative, the curvature term and the circumferential unit vector $\boldsymbol{\theta}_{j/i}$ in terms of the displacement functions $\boldsymbol{X}_i^{(2)}, \boldsymbol{X}_j^{(2)}$: Thus we obtain

$$\frac{\partial \boldsymbol{X}_i}{\partial t} = \frac{1}{\epsilon^2} \boldsymbol{X}_{i,\tau}^{(2)}, \tag{2.15}$$

where $\tau = t/\epsilon^4$. Next, using the relation

$$\kappa \boldsymbol{b} = \boldsymbol{t} \times \kappa \boldsymbol{n} = \boldsymbol{t} \times \boldsymbol{t}_{\tilde{s}}, \tag{2.16}$$

where $\tilde{s}$ is an arclength coordinate and $\boldsymbol{t}, \boldsymbol{n}, \boldsymbol{b}$ are the tangent, principal normal, and binormal unit vectors, and noticing that the straight-line coordinate s from (2.3) satisfies $s = \tilde{s}(1 + O(\epsilon^2))$ (see Klein & Majda 1991*a*), we find

$$(\kappa \boldsymbol{b})_i = \boldsymbol{t}_0 \times \boldsymbol{X}_{i,\sigma\sigma}^{(2)} + O(\epsilon) \tag{2.17}$$

(see (A 28) in the Appendix), where

$$\sigma = \frac{s}{\epsilon}. \tag{2.18}$$

Finally,

$$\boldsymbol{\theta}_{j/i} = \boldsymbol{t}_0 \times \frac{\boldsymbol{X}_i^{(2)} - \boldsymbol{X}_j^{(2)}}{|\boldsymbol{X}_i^{(2)} - \boldsymbol{X}_j^{(2)}|}, \tag{2.19}$$

(see (A 21), (A 7), (A 12) in the Appendix). Collecting (2.13)–(2.19), we arrive at the closed system of equations

$$\frac{\partial \boldsymbol{X}_i^{(2)}}{\partial \tau} = \frac{1}{4\pi} \boldsymbol{t}_0 \times \left\{ \alpha_i \Gamma_i \frac{\partial^2 \boldsymbol{X}_i^{(2)}}{\partial \sigma^2} + \sum_{j \neq i} 2\Gamma_j \frac{\boldsymbol{X}_i^{(2)} - \boldsymbol{X}_j^{(2)}}{|\boldsymbol{X}_i^{(2)} - \boldsymbol{X}_j^{(2)}|^2} \right\}, \tag{2.20}$$

which is equivalent to (1.2), except for a trivial rescaling of time by a factor of 4π and the choice $\boldsymbol{t}_0 = (0, 0, 1)$.

In the Appendix, we present an extended derivation of the dynamical equations for the evolution of N slender vortices that includes the first order in ϵ^2. Recovering (2.20) at the leading order, we demonstrate that the influence of non-local self-induction is in fact negligible as $\epsilon \to 0$ and the mutual induction acts only in a layered fashion in the present regime for geometrical perturbations of the vortices. It is nevertheless interesting to note the precise functional form of the non-local higher-order contributions for future reference, since their effects may become important for the longtime dynamics when the initial data do not lead to vortex collisions and breakdown of the solutions on the timescales considered here (see §§5.1 and 5.2 for solutions of (2.20) that do and do not exhibit local collisions of filaments in finite time, respectively).

3. Hamiltonian structure and conserved quantities

We write the simplified equations for interacting nearly parallel vortex filaments from (1.2) in the form,

$$\Gamma_j \frac{\partial \boldsymbol{X}_j}{\partial t} = J\left[\alpha_j \Gamma_j^2 \frac{\partial^2}{\partial \sigma^2} \boldsymbol{X}_j\right] + J\left[\sum_{k \neq j}^{N} 2\Gamma_j \Gamma_k \frac{(\boldsymbol{X}_j - \boldsymbol{X}_k)}{|\boldsymbol{X}_j - \boldsymbol{X}_k|^2}\right]. \tag{3.1}$$

In order to find the Hamiltonian for the system of equations in (3.1), we need to find a functional, $\mathscr{H}$, of the N-vortex filaments so that

$$\Gamma_j \frac{\partial \boldsymbol{X}_j}{\partial t} = J \frac{\delta \mathscr{H}}{\delta \boldsymbol{X}_j} \quad (1 \leqslant j \leqslant N). \tag{3.2}$$

In (3.2), $\delta\mathscr{H}/\delta \boldsymbol{X}_j$, denotes the functional or variational derivative (Logan 1987) with respect to the curvature $\boldsymbol{X}_j(\sigma)$ compared through the L^2 inner product for curves,

$$(\boldsymbol{\Phi}, \boldsymbol{\Psi})_0 = \int \boldsymbol{\Phi}(\sigma) \cdot \boldsymbol{\Psi}(\sigma)\, \mathrm{d}\sigma. \tag{3.3}$$

In (3.3) and the remainder of this paper we assume that the filament curves are either periodic in σ so that the integration range in (3.3) is over a period interval or that the filament curve perturbations vanish sufficiently rapidly together with their derivatives so that all the contributions from infinity vanish in the situation that the range of integration in (3.3) is the entire line.

To find the Hamiltonian satisfying (3.2) we write $\mathscr{H}$ in the form

$$\mathscr{H} = \mathscr{H}_s + \mathscr{H}_p \tag{3.4}$$

where, from (3.1)

$$\frac{\delta \mathscr{H}_s}{\delta \boldsymbol{X}_j} = \alpha_j \Gamma_j^2 \frac{\partial^2}{\partial \sigma^2} \boldsymbol{X}_j, \tag{3.5}$$

and

$$\frac{\delta \mathscr{H}_p}{\delta \boldsymbol{X}_j} = \sum_{k \neq j}^{N} 2\Gamma_j \Gamma_k \frac{(\boldsymbol{X}_j - \boldsymbol{X}_k)}{|\boldsymbol{X}_j - \boldsymbol{X}_k|^2}, \tag{3.6}$$

for $1 \leqslant j \leqslant N$. The functional, $\mathscr{H}_s$, satisfying (3.5) is given by

$$\mathscr{H}_s = -\sum_{j=1}^{N} \tfrac{1}{2}(\alpha_j \Gamma_j^2) \int \left| \frac{\partial \boldsymbol{X}_j}{\partial \sigma} \right|^2 \mathrm{d}\sigma, \tag{3.7}$$

while the functional, $\mathscr{H}_p$, satisfying (3.6) is merely the integral over σ of the familiar N-point vortex Hamiltonian (Lamb 1932), i.e.

$$\mathscr{H}_p = 2 \sum_{j<k}^{N} \int \Gamma_j \Gamma_k \ln |\boldsymbol{X}_j(\sigma) - \boldsymbol{X}_k(\sigma)|\, \mathrm{d}\sigma. \tag{3.8}$$

With (3.3)–(3.8), we conclude that the Hamiltonian satisfying (3.2) is given by

$$\mathscr{H} = -\sum_{j=1}^{N} \tfrac{1}{2}(\alpha_j \Gamma_j^2) \int \left| \frac{\partial \boldsymbol{X}_j}{\partial \sigma} \right|^2 \mathrm{d}\sigma + 2 \sum_{j<k}^{N} \int \Gamma_j \Gamma_k \ln |\boldsymbol{X}_j(\sigma) - \boldsymbol{X}_k(\sigma)|\, \mathrm{d}\sigma. \tag{3.9}$$

Of course, it follows immediately from the equations in (3.2), that

> the Hamiltonian, $\mathscr{H}$, is conserved in time for solutions of the asymptotic filament equations in (3.1). (3.10)

3.1. *Other conserved quantities*

The equations in (3.1) have other symmetries which lead to integrated analogues for solutions of (3.1) of the conservation of the centre of vorticity and angular momentum which are probably familiar to the reader for two-dimensional point vortices (Lamb 1932).

The Hamiltonian in (3.9) remains unchanged under the transformations $\boldsymbol{X}_j \mapsto \boldsymbol{X}_j + \boldsymbol{Z}_0$ where $\boldsymbol{Z}_0$ is an arbitrary 2-vector. Thus, we define the mean centre of vorticity by

$$\boldsymbol{M} = \int \sum_{j=1}^{N} \Gamma_j \boldsymbol{X}_j(\sigma)\, \mathrm{d}\sigma. \tag{3.11}$$

An elementary calculation establishes that $\mathrm{d}\boldsymbol{M}/\mathrm{d}t = 0$ for solutions of (3.1) so that

the mean centre of vorticity, $\boldsymbol{M}$, is
conserved in time for solutions of (3.1). (3.12)

Similarly, the Hamiltonian in (3.9) remains invariant under the transformations $\boldsymbol{X}_j \mapsto O(\theta)\boldsymbol{X}_j$ where $O(\theta)$ is an arbitrary rotation matrix. We define the mean angular momentum by

$$A = \int \sum_{j=1}^{N} \Gamma_j |\boldsymbol{X}_j(\sigma)|^2 \, \mathrm{d}\sigma \tag{3.13}$$

and elementary calculations establish that

the mean angular momentum, A, defined in
(3.13) is conserved in time for solutions of (3.1). (3.14)

There is another conserved quantity which arises for solutions of the interacting filament equations which is not derived as a direct analogue in integrated form from the equations for two-dimensional point vortices. The Hamiltonian in (3.9) remains invariant under the translation, $\boldsymbol{X}_j(\sigma) \mapsto \boldsymbol{X}_j(\sigma + h)$ where h is arbitrary so that Noether's theorem guarantees that there is another conserved quantity. By following the procedure for Noether's theorem in the form stated in Arnold (1989), we claim that the quantity

$$W = \int \sum_{j=1}^{N} \Gamma_j (J\boldsymbol{X}_j(\sigma)) \cdot \frac{\partial \boldsymbol{X}_j(\sigma)}{\partial \sigma} \mathrm{d}\sigma \tag{3.15}$$

is conserved in time for solutions of the filament equations in (3.1). To verify this, we calculate that

$$\begin{aligned} \frac{\mathrm{d}W}{\mathrm{d}t} &= 2 \int \sum_{j=1}^{N} \Gamma_j J \frac{\mathrm{d}\boldsymbol{X}_j}{\mathrm{d}t} \cdot \frac{\partial \boldsymbol{X}_j}{\partial \sigma} \mathrm{d}\sigma \\ &= \left\{ -2 \int \left(\sum_{j=1}^{N} \Gamma_j^2 \alpha_j \frac{\partial^2 \boldsymbol{X}_j}{\partial \sigma^2} \cdot \frac{\partial \boldsymbol{X}_j}{\partial \sigma} \right) \mathrm{d}\sigma \right\} \\ &\quad + \left\{ -4 \int \left(\sum_{j<k} \Gamma_j \Gamma_k \frac{\boldsymbol{X}_j - \boldsymbol{X}_k}{|\boldsymbol{X}_j - \boldsymbol{X}_k|^2} \cdot \frac{\partial}{\partial \sigma} (\boldsymbol{X}_j - \boldsymbol{X}_k) \right) \mathrm{d}\sigma \right\} \\ &= \{1\} + \{2\}. \end{aligned} \tag{3.16}$$

We claim that all of the integrands in both terms {1} and {2} are perfect derivatives so that all contributions on the right-hand side of (3.16) vanish. Since

$$2 \frac{\partial^2 \boldsymbol{X}_j}{\partial \sigma^2} \cdot \frac{\partial \boldsymbol{X}_j}{\partial \sigma} = \frac{\partial}{\partial \sigma} \left(\left| \frac{\partial \boldsymbol{X}_j}{\partial \sigma} \right|^2 \right),$$

the integrand in {1} is a perfect derivative while

$$\frac{\boldsymbol{X}_j - \boldsymbol{X}_k}{|\boldsymbol{X}_j - \boldsymbol{X}_k|^2} \cdot \frac{\partial}{\partial \sigma} (\boldsymbol{X}_j - \boldsymbol{X}_k) = \frac{\partial}{\partial \sigma} \ln |\boldsymbol{X}_j - \boldsymbol{X}_k|,$$

so that the integrand in {2} is also a perfect derivative. Thus,

the quantity, W, defined in (3.15) is conserved by
solutions of the filament equations in (3.1). (3.17)

3.2. *The average distance functional*

We briefly consider a generalized distance functional, I, defined by

$$I = \frac{1}{2}\int \sum_{j,k} \Gamma_j \Gamma_k |\boldsymbol{X}_j - \boldsymbol{X}_k|^2 \, \mathrm{d}\sigma. \tag{3.18}$$

We show below that I is conserved for special configurations consisting of identical vortex filaments. Through integration by parts, we compute in general that

$$\begin{aligned} \frac{\mathrm{d}I}{\mathrm{d}t} &= -\int \sum_{j,k}^{N} \left[\Gamma_j \boldsymbol{X}_j \cdot \Gamma_k \frac{\mathrm{d}\boldsymbol{X}_k}{\mathrm{d}t} + \Gamma_k \boldsymbol{X}_k \cdot \Gamma_j \frac{\mathrm{d}\boldsymbol{X}_j}{\mathrm{d}t} \right] \mathrm{d}\sigma \\ &= -\sum_{j,k}^{N} \Gamma_j \Gamma_k (\Gamma_k \alpha_k - \Gamma_j \alpha_j) \int \left(\frac{\partial x_j}{\partial \sigma}\frac{\partial y_k}{\partial \sigma} - \frac{\partial x_k}{\partial \sigma}\frac{\partial y_j}{\partial \sigma} \right) \mathrm{d}\sigma, \end{aligned} \tag{3.19}$$

where $\boldsymbol{X}_j(\sigma, t) = (x_j(\sigma, t), y_j(\sigma, t))$. From the identity in (3.19), we observe that

the average distance functional, I, is conserved in time for
solutions of (3.1) provided that the product of the circulation, Γ_j,
and the vortex structure parameter, α_j, is invariant
for all the filaments, i.e. $\Gamma_j \alpha_j = \Gamma_k \alpha_k$. (3.20)

In particular, for co-rotating filament pairs with the same structure in the vortex core, the distance functional, I, is conserved.

4. The equations for pairs of interacting filaments

Here we begin the study of solutions of the simplified equations for interacting filaments from (1.2) in the special case involving two interacting nearly parallel vortex filaments. For simplicity in exposition, we assume that the vortex core parameters α_j are identical and without loss of generality (by trivial time rescaling) we assume that one of the filaments has circulation, $\Gamma_1 = 1$, while the other vortex filament has circulation $\Gamma_2 = \Gamma$ where Γ satisfies $-1 \leqslant \Gamma \leqslant 1$ with $\Gamma \neq 0$; thus, Γ represents the circulation ratio of the two interacting filaments. For the pair of interacting filaments with $\boldsymbol{X}_j(\sigma, t) = (x_j, y_j)$, it will be convenient to introduce the complex coordinates for each filament

$$\psi_j = x_j(\sigma, t) + \mathrm{i} y_j(\sigma, t), \tag{4.1}$$

for $j = 1, 2$ with $\mathrm{i} = (-1)^{1/2}$.

With the simplification mentioned in the above paragraph, the equations in (1.2) specialized to the case of two interacting filaments have the form

$$\left.\begin{aligned} \frac{1}{\mathrm{i}}\frac{\partial \psi_1}{\partial t} &= \frac{\partial^2 \psi_1}{\partial \sigma^2} + 2\Gamma \frac{\psi_1 - \psi_2}{|\psi_1 - \psi_2|^2}, \\ \frac{1}{\mathrm{i}}\frac{\partial \psi_2}{\partial t} &= \Gamma \frac{\partial^2 \psi_2}{\partial \sigma^2} - 2\frac{\psi_1 - \psi_2}{|\psi_1 - \psi_2|^2}. \end{aligned}\right\} \tag{4.2}$$

From §3 these equations have the following conserved quantities,

$$\left.\begin{aligned} H &= -\frac{1}{2}\int\left|\frac{\partial\psi_1}{\partial\sigma}\right|^2 \mathrm{d}\sigma - \frac{\Gamma^2}{2}\int\left|\frac{\partial\psi_2}{\partial\sigma}\right|^2 \mathrm{d}\sigma + 2\left[\int \Gamma \ln|\psi_1-\psi_2|\,\mathrm{d}\sigma\right], \\ M &= \int\psi_1\,\mathrm{d}\sigma + \int\Gamma\psi_2\,\mathrm{d}\sigma, \\ A &= \int|\psi_1|^2\,\mathrm{d}\sigma + \int\Gamma|\psi_2|^2\,\mathrm{d}\sigma, \\ W &= \mathrm{i}\int\psi_1\frac{\partial\bar{\psi}_1}{\partial\sigma} + \Gamma\psi_2\frac{\partial\bar{\psi}_2}{\partial\sigma}\,\mathrm{d}\sigma. \end{aligned}\right\} \tag{4.3}$$

Furthermore, for corotating pairs so that $\Gamma = 1$, we have the additional conserved quantity

$$I = \int|\psi_1-\psi_2|^2\,\mathrm{d}\sigma. \tag{4.4}$$

To make the nonlinear term in (4.2) a function of only one variable we introduce the coordinates $\psi = \psi_1 - \psi_2$, and $\phi = \psi_1 + \psi_2$ so that

$$\left.\begin{aligned} \psi_1 &= \tfrac{1}{2}(\phi+\psi), \\ \psi_2 &= \tfrac{1}{2}(\phi-\psi). \end{aligned}\right\} \tag{4.5}$$

The equations in (4.2) have the following form in the new variables,

$$\left.\begin{aligned} \frac{1}{\mathrm{i}}\phi_t &= \tfrac{1}{2}(1+\Gamma)\,\phi_{\sigma\sigma} + \tfrac{1}{2}(1-\Gamma)\left[\psi_{\sigma\sigma} - 4\frac{\psi}{|\psi|^2}\right], \\ \frac{1}{\mathrm{i}}\psi_t &= \tfrac{1}{2}(1-\Gamma)\,\phi_{\sigma\sigma} + \tfrac{1}{2}(1+\Gamma)\left[\psi_{\sigma\sigma} + 4\frac{\psi}{|\psi|^2}\right]. \end{aligned}\right\} \tag{4.6}$$

4.1. *Corotating filament pairs*

For corotating filament pairs with $\Gamma = 1$, the two equations in (4.6) completely decouple into two separate scalar equations given by

$$\left.\begin{aligned} \frac{1}{\mathrm{i}}\phi_t &= \phi_{\sigma\sigma}, \\ \frac{1}{\mathrm{i}}\psi_t &= \psi_{\sigma\sigma} + \frac{4\psi}{|\psi|^2}. \end{aligned}\right\} \tag{4.7}$$

The first equation in (4.7) is the linear Schrödinger equation while the second equation in (4.7) is a nonlinear Schrödinger equation with an unusual nonlinearity.

The equations in (4.7) have a dispersive wavelike behaviour. We demonstrate this by writing down some elementary exact solutions by following a standard procedure (Klein & Majda 1991*b*). The complex function ψ will be a nonlinear plane wave solution of the form

$$\psi = B\,\mathrm{e}^{\mathrm{i}(k\sigma+\omega t)}, \tag{4.8}$$

provided that

$$\omega = \frac{4}{B^2} - k^2. \tag{4.9}$$

With these exact solutions, we obtain general wavelike solutions in the original complex filament coordinates given by

$$\left.\begin{aligned}\psi_1 &= \phi(\sigma,t)+\tfrac{1}{2}B\,\mathrm{e}^{\mathrm{i}(k\sigma+\omega t)},\\ \psi_2 &= \phi(\sigma,t)-\tfrac{1}{2}B\,\mathrm{e}^{\mathrm{i}(k\sigma+\omega t)},\end{aligned}\right\} \tag{4.10}$$

where ϕ is an arbitrary solution of the linear Schrödinger equation. The numerical experiments reported in §5 confirm the wavelike behaviour of general solutions of the corotating filament pair.

4.2. *Zakharov's equation for counter-rotating symmetric filaments*

For counter-rotating vortex filaments with $\Gamma = -1$, the filament equations from (4.6) are strongly coupled and are given by

$$\left.\begin{aligned}\frac{1}{\mathrm{i}}\phi_t &= \psi_{\sigma\sigma}-4\frac{\psi}{|\psi|^2},\\ \frac{1}{\mathrm{i}}\psi_t &= \phi_{\sigma\sigma}.\end{aligned}\right\} \tag{4.11}$$

Symmetric perturbations of the counter-rotating filament pair in the sense of Crow (1970) (also see Klein & Majda 1993) produce special nonlinear solutions of the filament equations in (4.2) with $\Gamma = -1$ which satisfy the symmetric conditions

$$\psi_2(\sigma,t) = -\bar{\psi}_1(\sigma,t), \tag{4.12}$$

for all times. With (4.5) and the symmetry conditions in (4.12), we have $\phi = 2\mathrm{i}\,\mathrm{Im}\,\psi_1$ and $\psi = \mathrm{Re}\,\psi_1$. Thus, with the definition $\psi_1(\sigma,t) = u(\sigma,t)-\mathrm{i}v(\sigma,t)$, the two complex-valued equations in (4.11) reduce, for symmetric perturbations, to the two coupled real equations

$$\left.\begin{aligned}v_t &= -u_{\sigma\sigma}+\frac{1}{u},\\ u_t &= v_{\sigma\sigma}.\end{aligned}\right\} \tag{4.13}$$

Without presenting any details, Zakharov (1988) wrote down the equations

$$\left.\begin{aligned}v_t &= -\alpha(u)\,u_{\sigma\sigma}+\frac{1}{u},\\ u_t &= \alpha(u)\,v_{\sigma\sigma},\end{aligned}\right\} \tag{4.14}$$

with the nonlinear coefficient, $\alpha(u) = \ln(u/d)$, and proposed the solutions of these equations as a model for the collapse of symmetric perturbations of the counter-rotating vortex pair. The equation in (4.13) is essentially Zakharov's proposed equation in (4.14) except that the peculiar logarithmic dependence of $\alpha(u)$ in (4.14) has been replaced by a constant. Furthermore, the equation in (4.13) has been derived through self-consistent asymptotic principles as presented in §2 followed by the straightforward calculations from this section which exploit the very special circumstances involving symmetric perturbations of the counter-rotating pair.

4.3. *Linearized stability theory for the filament pair*

Here we investigate the linearized stability of the straight-line two-dimensional point-vortex solutions for any arbitrary circulation ratio within the class of all filament perturbations which satisfy the simplified asymptotic equations in (4.2).

We choose the origin of our coordinates so that at time $t = 0, \psi_1 = (\frac{1}{2}d, 0)$ and $\psi_2 = (-\frac{1}{2}d, 0)$ where d is the separation distance. With the variables ϕ and ψ satisfying the transformed filament equations in (4.6), we write down the familiar exact solutions (Lamb 1932) that correspond to pairs of straight-line point vortex solutions with the explicit formulas for $\Gamma \neq -1$,

$$\left.\begin{aligned} \phi^{(0)}(t) &= 2\frac{(\psi_1(0)+\Gamma\psi_2(0))}{(1+\Gamma)}+\frac{(\Gamma-1)}{(\Gamma+1)}d\exp\left(\frac{2\mathrm{i}(1+\Gamma)t}{d^2}\right), \\ &= d\left(1-\exp\left(\frac{2\mathrm{i}(1+\Gamma)t}{d^2}\right)\right)\frac{(1-\Gamma)}{(1+\Gamma)}, \\ \psi^{(0)}(t) &= d\exp\left(\frac{2(1+\Gamma)t}{d^2}\right), \end{aligned}\right\} \tag{4.15}$$

and for $\Gamma = -1$,

$$\left.\begin{aligned} \phi^{(0)}(t) &= -\frac{4\mathrm{i}}{d^2}t, \\ \psi^{(0)}(t) &= (d, 0). \end{aligned}\right\} \tag{4.16}$$

We linearize the equations in (4.6) about these exact solutions ϕ^0, ψ^0 and obtain the linearized equations for perturbations, still denoted by ϕ and ψ, and given by

$$\left.\begin{aligned} \frac{\partial\phi}{\partial t} &= \tfrac{1}{2}\mathrm{i}(1+\Gamma)\phi_{\sigma\sigma}+\tfrac{1}{2}(1-\Gamma)\left[\psi_{\sigma\sigma}+4\frac{\bar{\psi}}{\bar{\psi}_0^2}\right], \\ \frac{\partial\psi}{\partial t} &= \tfrac{1}{2}\mathrm{i}(1-\Gamma)\phi_{\sigma\sigma}+\tfrac{1}{2}(1+\Gamma)\left[\psi_{\sigma\sigma}-4\frac{\bar{\psi}}{\bar{\psi}_0^2}\right], \end{aligned}\right\} \tag{4.17}$$

where $\psi_0 = d\exp(2\mathrm{i}(1+\Gamma)t/d^2)$ and a bar indicates complex conjugation. To get rid of the time dependence that enters through $\bar{\psi}_0^2$, we go to a coordinate frame that rotates with the vortex filaments, through the variables χ and Θ defined by

$$\left.\begin{aligned} \chi(\sigma, t) &= \psi(\sigma, t)\exp(-2\mathrm{i}(1+\Gamma)t/d^2), \\ \Theta(\sigma, t) &= \phi(\sigma, t)\exp(-2\mathrm{i}(1+\Gamma)t/d^2). \end{aligned}\right\} \tag{4.18}$$

With this transformation, the linearized equations of motion and the equations for the corresponding complex conjugates are given by

$$\left.\begin{aligned} \frac{1}{\mathrm{i}}\chi_t &= \tfrac{1}{2}(1+\Gamma)\left[\chi_{\sigma\sigma}-\frac{4}{d^2}\chi\right]+\tfrac{1}{2}(1-\Gamma)\Theta_{\sigma\sigma}-\frac{2(1+\Gamma)}{d^2}\bar{\chi}, \\ \frac{1}{\mathrm{i}}\Theta_t &= \tfrac{1}{2}(1-\Gamma)\chi_{\sigma\sigma}+\tfrac{1}{2}(1+\Gamma)\left[\Theta_{\sigma\sigma}-\frac{4}{d^2}\Theta\right]+\frac{2(1-\Gamma)}{d^2}\bar{\chi}, \\ \frac{1}{\mathrm{i}}\bar{\chi}_t &= -\tfrac{1}{2}(1+\Gamma)\left[\bar{\chi}_{\sigma\sigma}-\frac{4}{d^2}\bar{\chi}\right]-\tfrac{1}{2}(1-\Gamma)\bar{\Theta}_{\sigma\sigma}+\frac{2(1+\Gamma)}{d^2}\chi, \\ \frac{1}{\mathrm{i}}\bar{\Theta}_t &= -\tfrac{1}{2}(1-\Gamma)\bar{\chi}_{\sigma\sigma}-\tfrac{1}{2}(1+\Gamma)\left[\bar{\Theta}_{\sigma\sigma}-\frac{4}{d^2}\bar{\Theta}\right]-\frac{2(1-\Gamma)}{d^2}\chi. \end{aligned}\right\} \tag{4.19}$$

We solve this 4×4 system with the Fourier transform. The coupling of χ and Θ to their complex conjugates, $\bar{\chi}$ and $\bar{\Theta}$, in real space means that $\hat{\chi}(\xi, t)$ is coupled to $\bar{\hat{\chi}}(-\xi, t)$ in wavenumber space and the same is true for Θ where ξ is the wavenumber. In

wavenumber space the equations in (4.19) reduce to the 4×4 matrix-ordinary differential equation,

$$\frac{\mathrm{d}}{\mathrm{d}t}\begin{pmatrix}\hat{\chi}(\xi,t)\\ \hat{\Theta}(\xi,t)\\ \bar{\hat{\chi}}(-\xi,t)\\ \bar{\hat{\Theta}}(-\xi,t)\end{pmatrix} = \mathrm{i}A(\xi)\begin{pmatrix}\hat{\chi}(\xi,t)\\ \hat{\Theta}(\xi,t)\\ \bar{\hat{\chi}}(-\xi,t)\\ \bar{\hat{\Theta}}(-\xi,t)\end{pmatrix}, \tag{4.20}$$

where

$$A(\xi) = \begin{pmatrix} -\frac{1}{2}(1+\Gamma)\left(\xi^2+\frac{4}{d^2}\right) & -\frac{1}{2}(1-\Gamma)\xi^2 & -\frac{2(1+\Gamma)}{d^2} & 0\\ -\frac{1}{2}(1-\Gamma)\xi^2 & -\frac{1}{2}(1+\Gamma)\left(\xi^2+\frac{4}{d^2}\right) & \frac{2(1-\Gamma)}{d^2} & 0\\ \frac{2(1+\Gamma)}{d^2} & 0 & \frac{1}{2}(1+\Gamma)\left(\xi^2+\frac{4}{d^2}\right) & \frac{1}{2}(1-\Gamma)\xi^2\\ -\frac{2(1-\Gamma)}{d^2} & 0 & \frac{1}{2}(1-\Gamma)\xi^2 & \frac{1}{2}(1+\Gamma)\left(\xi^2+\frac{4}{d^2}\right)\end{pmatrix}. \tag{4.21}$$

The matrix $A(\xi)$ has the eigenvalues $\lambda^1_\pm = \pm\frac{1}{2}(\mathscr{R}+2\mathscr{P}^{1/2})^{1/2}$ and $\lambda^2_\pm = \pm\frac{1}{2}(\mathscr{R}-2\mathscr{P}^{1/2})^{1/2}$, where

$$\left.\begin{aligned}\mathscr{R} &= 8\frac{a^2}{d^4}+8\frac{a^2\xi^4}{d^2}+a^2\xi^4+b^2\xi^4,\\ \mathscr{P} &= 16\frac{a^4}{d^8}+32\frac{a^2b^2\xi^2}{d^6}+20\frac{a^2b^2\xi^4}{d^4}+4\frac{b^4\xi^4}{d^4}+8\frac{a^2b^2\xi^6}{d^2}+a^2b^2\xi^8,\end{aligned}\right\} \tag{4.22}$$

with $a = 1+\Gamma$ and $b = 1-\Gamma$. We have growing solutions and linearized instability whenever the $\lambda_\pm$ are imaginary. From the form of the $\lambda_\pm$ it is easy to see that since both $\mathscr{R}$ and $\mathscr{P}$ are positive real numbers from (4.22), $\lambda^1_\pm$ is always a real number. Thus, only $\lambda^2_\pm$, which has a minus sign under the radicand, can assume imaginary values and yield instability. It is useful to define the growth factor $\mathscr{G}$, which depends on the signs of the radicands in $\lambda^2_\pm$,

$$\mathscr{G} = \mathrm{sgn}\left(-(\mathscr{R}-2\mathscr{P}^{1/2})\right)|(\mathscr{R}-2\mathscr{P}^{1/2})^{1/2}|. \tag{4.23}$$

Whenever the $\lambda^2_\pm$ are real, $\mathscr{G}$ is negative, and the perturbations are neutrally stable with the oscillation frequency given by the absolute value of $\mathscr{G}$. If, however, any one of the $\lambda^2_\pm$ is imaginary, $\mathscr{G}$ is positive, and we have either exponentially growing and damped solutions, with the growth/damping rate given by the absolute value of $\mathscr{G}$. In general the growing solution dominates and we have an instability. From the definition of $\mathscr{G}$, we have $\mathscr{G} > 0$ and instability if and only if $\mathscr{R}^2 < 4\mathscr{P}$. Therefore we consider the quantity, $\mathscr{R}^2-4\mathscr{P}$, given explicitly from (4.22) by

$$\mathscr{Q} = \mathscr{R}^2-4\mathscr{P} = [a^2-b^2]\left[128\frac{a^2\xi^2}{d^6}+80\frac{a^2\xi^4}{d^4}+16\frac{b^2\xi^4}{d^2}+16\frac{a^2\xi^6}{d^2}+(a^2-b^2)\xi^8\right], \tag{4.24}$$

where as before $a = 1+\Gamma$ and $b = 1-\Gamma$.

First, we consider the situation with a positive circulation ratio so that $1 \geqslant \Gamma > 0$; in this case, we have the inequality $a > b$ which guarantees by (4.24) that $\mathscr{R}^2-4\mathscr{P}$ is positive for all wavenumbers ξ and there are no growing modes. Thus, we have linearized (neutral) stability for the vortex pair in this situation.

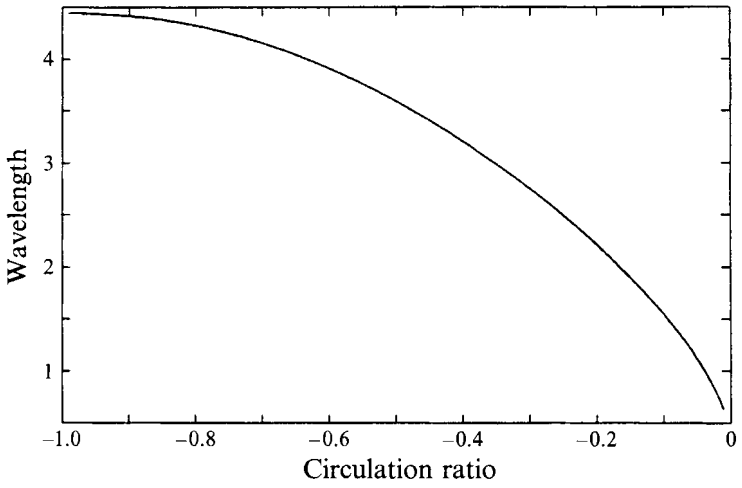

FIGURE 3. The wavelength of the most unstable mode predicted by linearized theory as a function of the circulation ratio Γ with $-1 \leqslant \Gamma < 0$ with separation distance, $d = 1$.

Next, we consider the situation with negative circulation ratios Γ with $-1 \leqslant \Gamma < 0$ which implies that we have $a < b$. From (4.24) in this case the only positive term in $\mathscr{Q} = \mathscr{R}^2 - 4\mathscr{P}$ is $(b^2 - a^2)\, b^2 \xi^8$. At long wavelengths, $\xi^2 \ll 1$, This positive term is dominated in magnitude by the negative contributions to $\mathscr{Q}$ of order ξ^2, ξ^4 and ξ^6; thus, there is always long-wavelength instability for the straight-line vortex pair for any negative circulation ratio. On the other hand, at short wavelengths, $\xi^2 \gg 1$, $\mathscr{R}^2 - 4\mathscr{P}$ is dominated by the positive factor $[a^2 - b^2]^2 \xi^8$ and there is always short-wavelength stability.

We summarize our analysis presented in the previous two paragraphs in the following fashion:

> Within the simplified vortex filament equations in (4.2), straight-line point-vortex pairs have linearized long-wavelength instability for arbitrary negative circulation ratios and linearized (neutral) stability for arbitrary positive circulation ratios. (4.25)

For any fixed negative circulation ratio, the graph of the stability function $\mathscr{G}$ from (4.23) is positive over a finite interval of wavenumbers extending from zero where $\mathscr{G}$ vanishes. For each negative circulation ratio there is a unique wavenumber with the largest growth rate and we plot the wavelength of this most unstable linearized mode versus the negative circulation ratio in figure 3 for a separation distance $d = 1$. Notice that as the circulation Γ tends to zero, this wavelength decreases to zero. The asymptotic derivation presented in §2 is valid for a fixed circulation ratio, Γ, but is not uniformly valid in the limit when $\Gamma \to 0$. The short-wavelength behaviour in figure 3 for the predictions from linear theory is one manifestation of this non-uniformity in the asymptotics.

4.4. *A numerical method for interacting filament pairs*

Here we briefly describe an accurate and robust method for the numerical solution of the filament pair equations in (4.2). We consider filament pairs that are 2π-periodic in σ. The overall strategy utilizes the method of splitting and is similar conceptually to the numerical procedure from Klein & Majda (1991*b*).

In one of the basic fractional steps, the point-vortex equations,

$$\left.\begin{aligned} \frac{1}{\mathrm{i}}\frac{\partial \psi_1}{\partial t} &= 2\Gamma\frac{\psi_1-\psi_2}{|\psi_1-\psi_2|^2}, \\ \frac{1}{\mathrm{i}}\frac{\partial \psi_2}{\partial t} &= -2\frac{\psi_1-\psi_2}{|\psi_1-\psi_2|^2}, \end{aligned}\right\} \tag{4.26}$$

are solved exactly through a timestep at a discrete number of evenly spaced spatial grid points through explicit solution formulae as presented in (4.15) and (4.16). In the other fractional step, the linear Schrödinger equations

$$\left.\begin{aligned} \frac{1}{\mathrm{i}}\frac{\partial \psi_1}{\partial t} &= \frac{\partial^2 \psi_1}{\partial \sigma^2}, \\ \frac{1}{\mathrm{i}}\frac{\partial \psi_2}{\partial t} &= \Gamma\frac{\partial^2 \psi_2}{\partial \sigma^2}, \end{aligned}\right\} \tag{4.27}$$

are solved exactly for a timestep via discrete fast Fourier transform and explicit exact solution in wavenumber space. These two steps are alternated in time in a standard fashion to yield second-order accuracy (Klein & Majda 1991*b*). Furthermore, this numerical method (4.3) exactly conserves in time the conserved quantities in (4.3) involving the mean centre of vorticity, $\boldsymbol{M}$, the mean angular momentum, A, and also the distance functional, I for the special case $\Gamma = 1$, since both of the separate fractional steps in (4.26) and (4.27) automatically conserve these quantities.

The Hamiltonian, $\mathscr{H}$, from (3.9) is not conserved exactly by the numerical procedure and we utilize the conservation of this quantity as an accuracy check on the timestep. We control the timestep by requiring conservation of the Hamiltonian to a precision of 1 in 10^5. for each simulation, when the error in the Hamiltonian (the deviation from the initial value) fluctuated by more than 10^{-5}, we reduced the timestep by a factor of five using a conditional if-then-else loop. The lower limit on the timestep in our variable timestep scheme was set at $\Delta t = 10^{-6}$.

We validated this numerical procedure by utilizing the exact solutions from §4.1 for $\Gamma = 1$ and also by comparison with the detailed predictions of the linearized theory from §4.3 at short times. Results based on these second validation tests will be presented at the beginning of the next section. All calculations reported in this paper used 256 nodes with some additional calculations involving 1024 nodes in spatial refinement studies for convergence. The minimal timestep size, $\Delta t = 10^{-6}$, for conservation of the Hamiltonian was never reached for all of the results reported in §5 until the critical time T_* where the filament pair exhibited finite-time collapse. We also used the Fourier energy spectrum of the solution as a numerical diagnostic for the spatial resolution (Klein & Majda 1991*b*). Even for the problems with finite-time collapse to be discussed in §5.1, the energy spectrum for each filament curve remained concentrated in the low wavenumbers typically smaller than 20 (Damodaran 1994) so that the computed solutions are well resolved with 256 Fourier modes.

5. Nonlinear behaviour and finite time collapse for interacting filament pairs

Here we present the detailed nonlinear behaviour of solutions of the simplified equations for interacting pairs of vortex filaments in (4.2).

5.1. *Nonlinear finite time collapse for any negative circulation ratio*

First, we explore the effects of nonlinearity as compared with the detailed predictions of linearized stability theory from §4.3 for the two representative negative circulation ratios, $\Gamma = -1.0, -0.5$. To calculate the nonlinear behaviour of solutions of (4.2) we use the numerical method described in §4.4 here and elsewhere in this section. Also, we normalize the separation distance of the unperturbed filament pair as $d = 1$ here and for any other circulation ratio used in this section.

We pick initial data which involve small perturbations of the straight-line filament pair with wavelength 2π which correspond to the eigenvector of the matrix $iA(\xi)$ from (4.20) associated with the eigenvalue yielding unstable growth for the wavenumber $\xi = 1$ according to the linear theory described earlier in §4.3. Thus, for the anti-parallel pair with $\Gamma = -1$, we consider initial data involving special symmetric perturbations (see (4.12) and Crow 1970) of the filament pair with the form

$$\left.\begin{aligned} \psi_1 &= -\tfrac{1}{2} + A\left(-\tfrac{1}{2} + \frac{1}{2\sqrt{3}}\mathrm{i}\right)(\mathrm{e}^{\mathrm{i}\sigma} - \mathrm{e}^{-\mathrm{i}\sigma}), \\ \psi_2 &= \tfrac{1}{2} + A\left(-\tfrac{1}{2} - \frac{1}{2\sqrt{3}}\mathrm{i}\right)(\mathrm{e}^{\mathrm{i}\sigma} - \mathrm{e}^{-\mathrm{i}\sigma}), \end{aligned}\right\} \tag{5.1}$$

where A is an amplitude parameter measuring the strength of the initial perturbation. For the filament pair with $\Gamma = -0.5$, the perturbations which are most unstable at wavelength 2π have the form

$$\left.\begin{aligned} \psi_1 &= -0.5 + A((0.061 - 0.237\mathrm{i})\,\mathrm{e}^{-\mathrm{i}\sigma} + (0.203 + 0.138\mathrm{i})\,\mathrm{e}^{\mathrm{i}\sigma}), \\ \psi_2 &= 0.5 + A((0.6 - 0.513\mathrm{i})\,\mathrm{e}^{-\mathrm{i}\sigma} + (0.79 + 0.011\mathrm{i})\,\mathrm{e}^{\mathrm{i}\sigma}). \end{aligned}\right\} \tag{5.2}$$

Here and elsewhere in this section, we monitor the minimum filament separation distance, $d_*(t)$, as a function of time where

$$d_*(t) = \min_{0 \leqslant \sigma \leqslant 2\pi} |\psi_1(\sigma, t) - \psi_2(\sigma, t)|.$$

Obviously, there is finite-time collapse of the filament pair provided $d_*(t)$ tends to zero as t approaches some finite time T_*.

With the small-amplitude perturbations for the initial data with $A = 0.03$ in (5.1) and (5.2) for $\Gamma = -1, -0.5$, respectively, in figure 4 we graph the time history of the minimal separation distance for the nonlinear solution of the filament pair equation from (4.2) and compare this behaviour with that predicted by the linearized theory from §4.3, i.e. using the time-dependent solution of the linear problem in (4.20). As expected, the predictions of linear theory and the nonlinear behaviour both agree for both circulation ratios for short times when the amplitude of the perturbation remains small. This agreement for the early time behaviour also indicates the accuracy of the numerical method described in §4.4. However, for both negative circulation ratios, the graphs in figure 4 indicate that as time evolves the nonlinear solutions exhibit finite-time collapse through substantial nonlinear behaviour. Next we document the geometric nature of this nonlinear collapse in detail for the two negative circulation ratios with several larger-amplitude initial perturbations of the filament pair.

Nonlinear collapse for $\Gamma = -1$

We consider initial data for the filament pair with $\Gamma = -1$ with the form in (5.1) but with a large perturbation amplitude adjusted so that the initial minimum separation distance was 0.4. The graph of the separation distance as a function of time, not

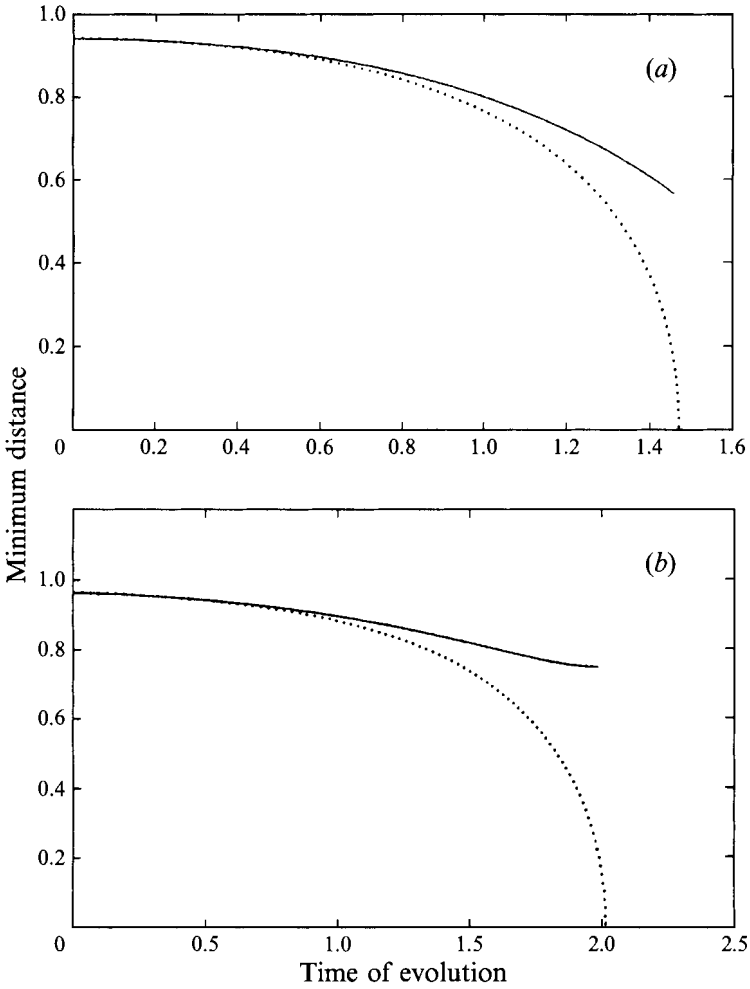

FIGURE 4. The minimum separation distance as a function of time with comparison of ..., nonlinear solution and ——, linearized solution (*a*) for $\Gamma = -1.0$ and (*b*) for $\Gamma = -0.5$.

displayed here, behaved qualitatively like that in figure 4(*a*) with a much earlier time for filament collapse, $t = 0.1146$, owing to the larger amplitude of this perturbation along the unstable eigenmode. In figures 5–7 we display snapshots of the solution of the filament equations in (4.2) with this initial data for times $t = 0$, 0.0800, 0.1146 as it evolves toward collapse. In these as well as in subsequent figures in this section, we display both a three-dimensional perspective of the two filament curves and also projections of these filament curves along the three coordinate planes. The initial perturbations are symmetric for the anti-parallel pair and, as expected from §4.2, the solutions retain this symmetry throughout the nonlinear evolution. The nature of the filament collapse presented in these figures is very intuitive when one considers the behaviour locally of point vortices in two dimensions with equal and opposite circulations summarized in (4.16) above. As figures 5–7 indicate, the points of closest separation move more rapidly and pinch off faster than the rest of the vortex filament and the magnitude of the pinching necessarily increases dramatically as the interaction with the linearized local self-induction represented in (4.2) brings the filaments together. The result of this interaction is finite-time collapse.

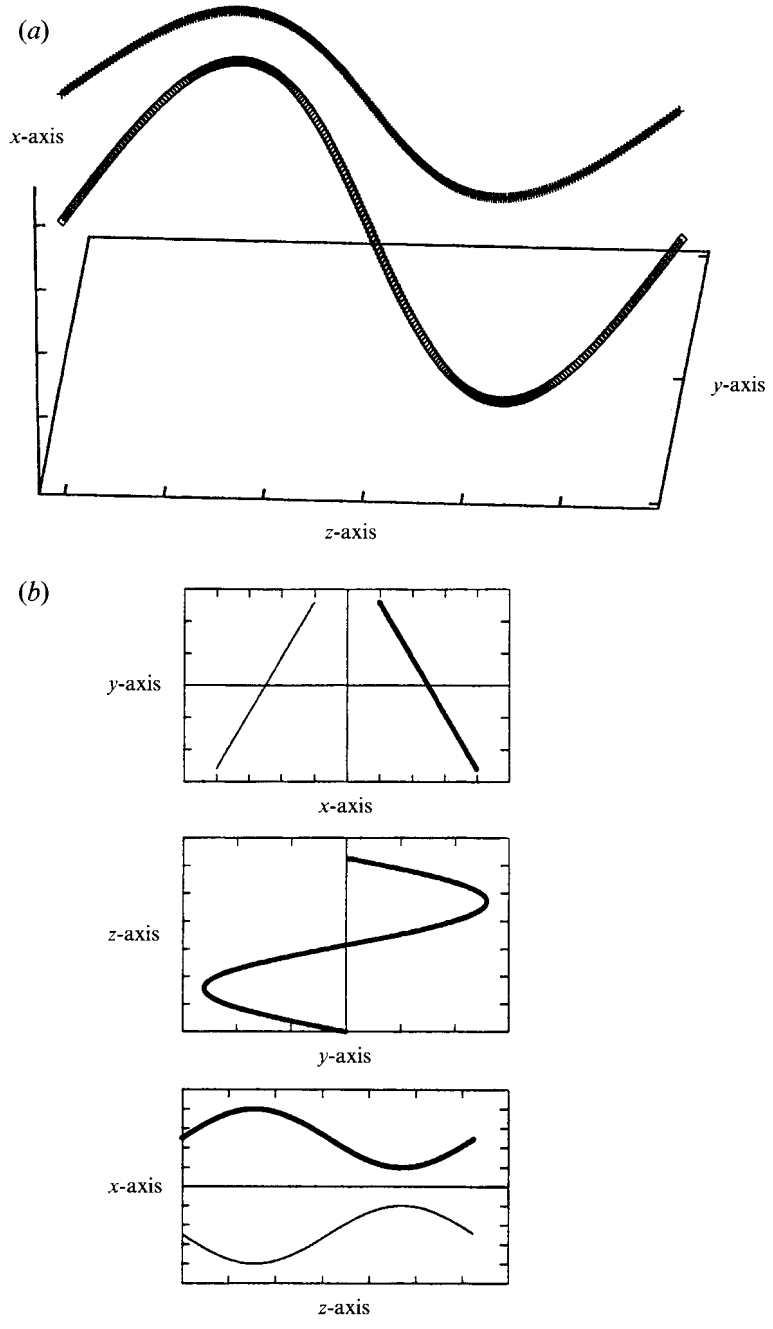

FIGURE 5. Snapshot of filaments for symmetric perturbation and $\Gamma = -1$ at time $t = 0$; (*b*) is the projection of the filaments on the coordinate axes.

In the next numerical experiment described here, we consider large-amplitude antisymmetric helical initial perturbations of the anti-parallel pair (Crow 1970) given by

$$\left.\begin{aligned} \psi_1 &= -0.5 + 0.3\,\mathrm{e}^{\mathrm{i}\sigma}, \\ \psi_2 &= 0.5 + 0.3\,\mathrm{e}^{\mathrm{i}\sigma}. \end{aligned}\right\} \tag{5.3}$$

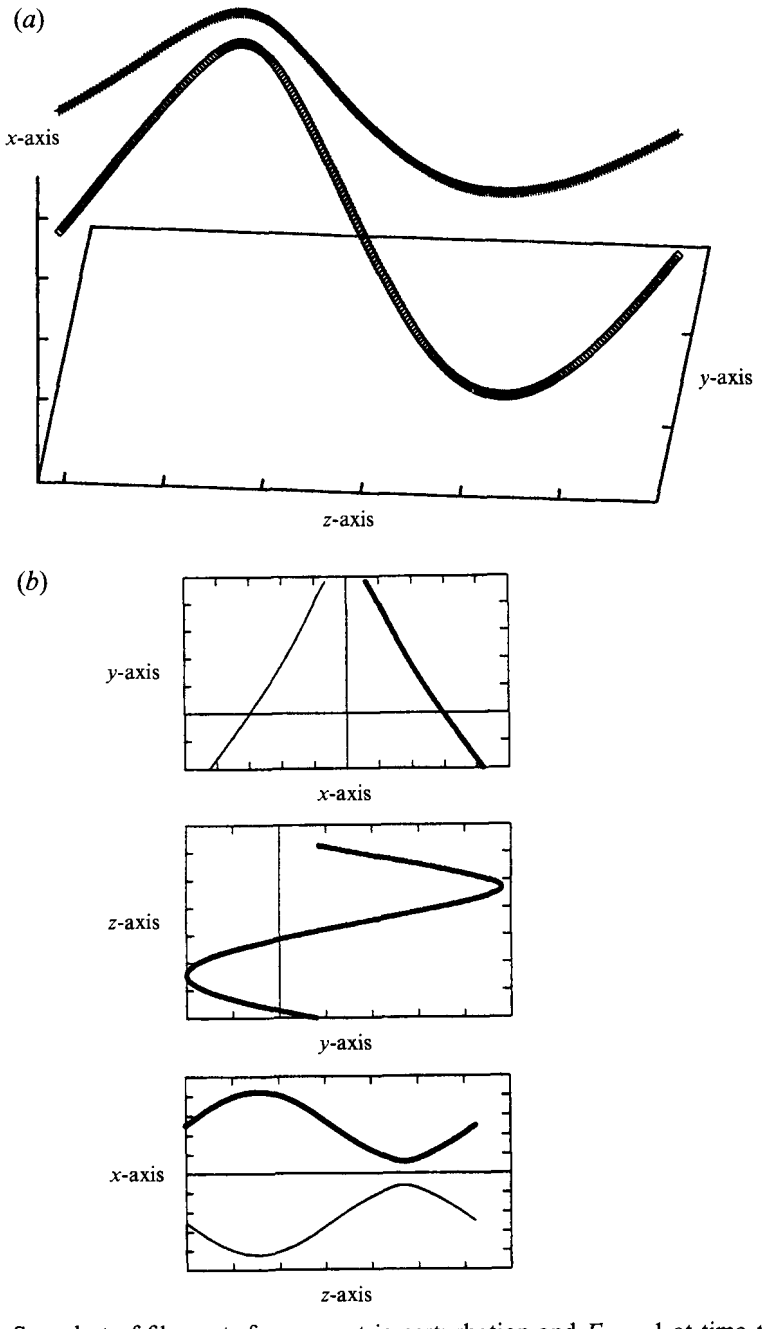

FIGURE 6. Snapshot of filaments for symmetric perturbation and $\Gamma = -1$ at time $t = 0.0800$.

Clearly, for such antisymmetric perturbations, the initial separation distance between the two filaments is identically constant. Furthermore, as regards the linearized theory from §4.3, antisymmetric perturbations for the circulation ratio $\Gamma = -1$ are neutrally stable and do not grow in time. Despite this fact, the nonlinear solution of the filament pair equations with this initial data exhibits finite-time collapse at $t = 0.7068$ and the graph of the minimum separation distance, $d_*(t)$ is a monotome decreasing function of time which resembles that in figure 4(*a*). Snapshots of the evolving filament curves at

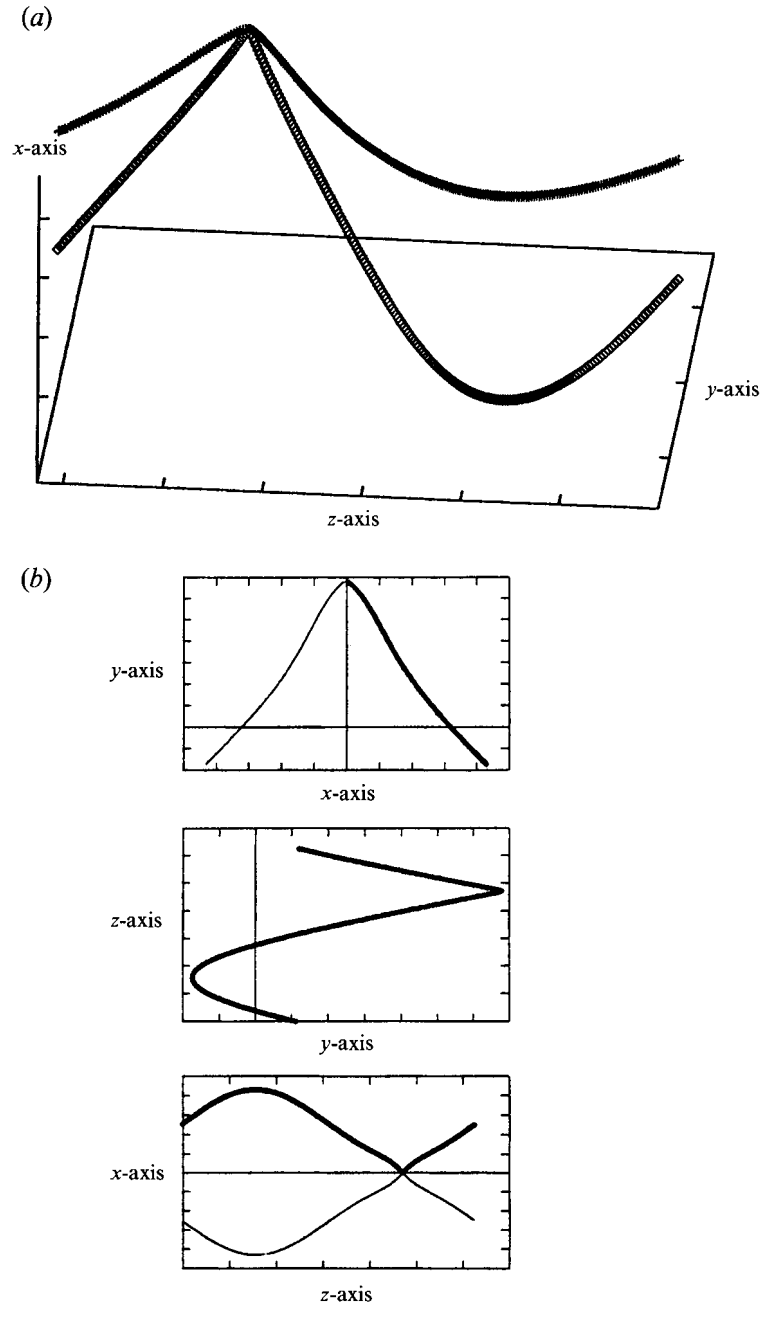

FIGURE 7. Snapshot of filaments for symmetric perturbation and $\Gamma = -1$ at time $t = 0.1146$.

times $t = 0$, 0.67 and 0.7068 are given in figures 8, 9 and 10, respectively. One striking feature of the nonlinear collapse is that the filament curves initially are antisymmetric about the line between them as depicted in figure 8, but at the collapse time they are almost symmetric about the same line as indicated in figure 10. In fact, it is clear from comparing figures 9 and 10 with figures 6 and 7 that locally the nonlinear collapse strongly resembles the symmetric collapse discussed in detail previously. These two examples give convincing evidence that general perturbations of the anti-parallel pair

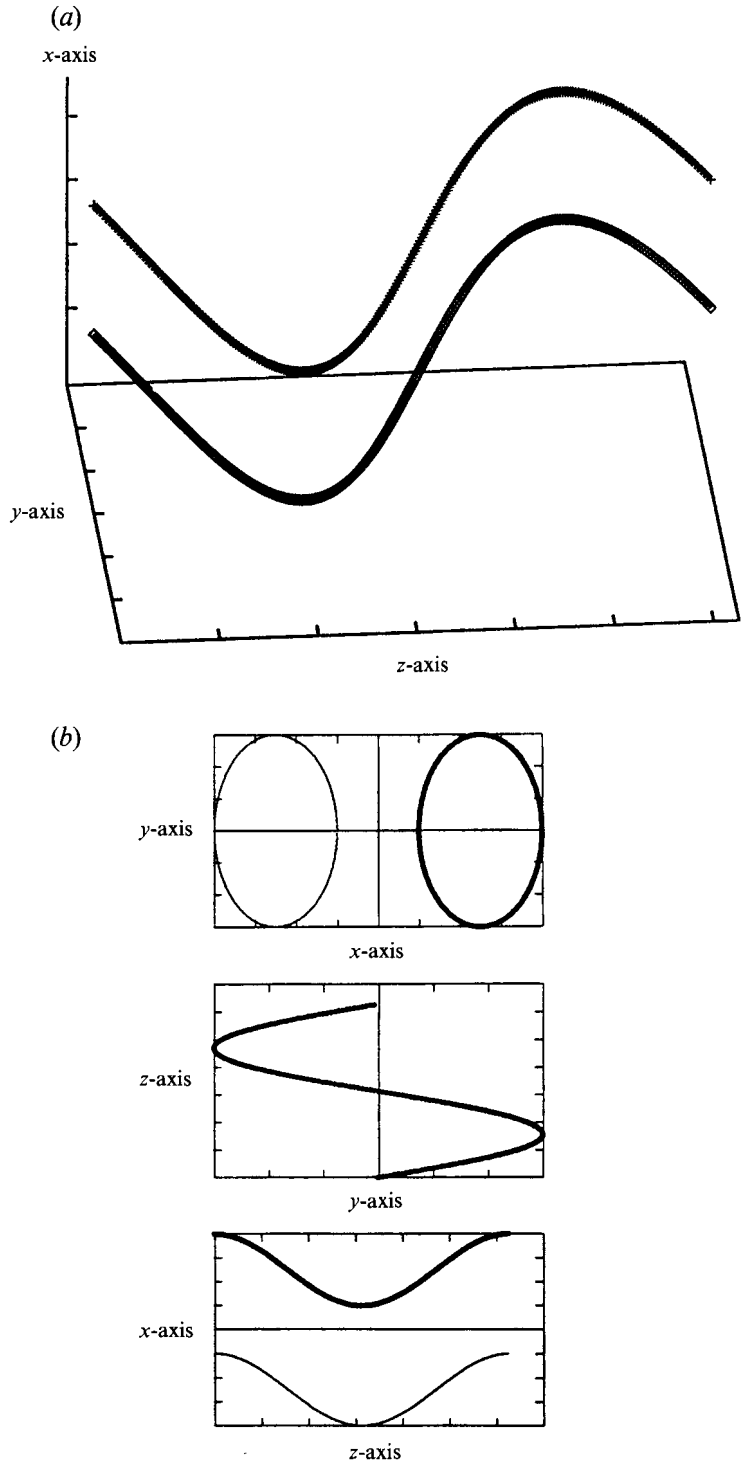

FIGURE 8. Snapshot of filaments for antisymmetric perturbation and $\Gamma = -1$ at time $t = 0$.

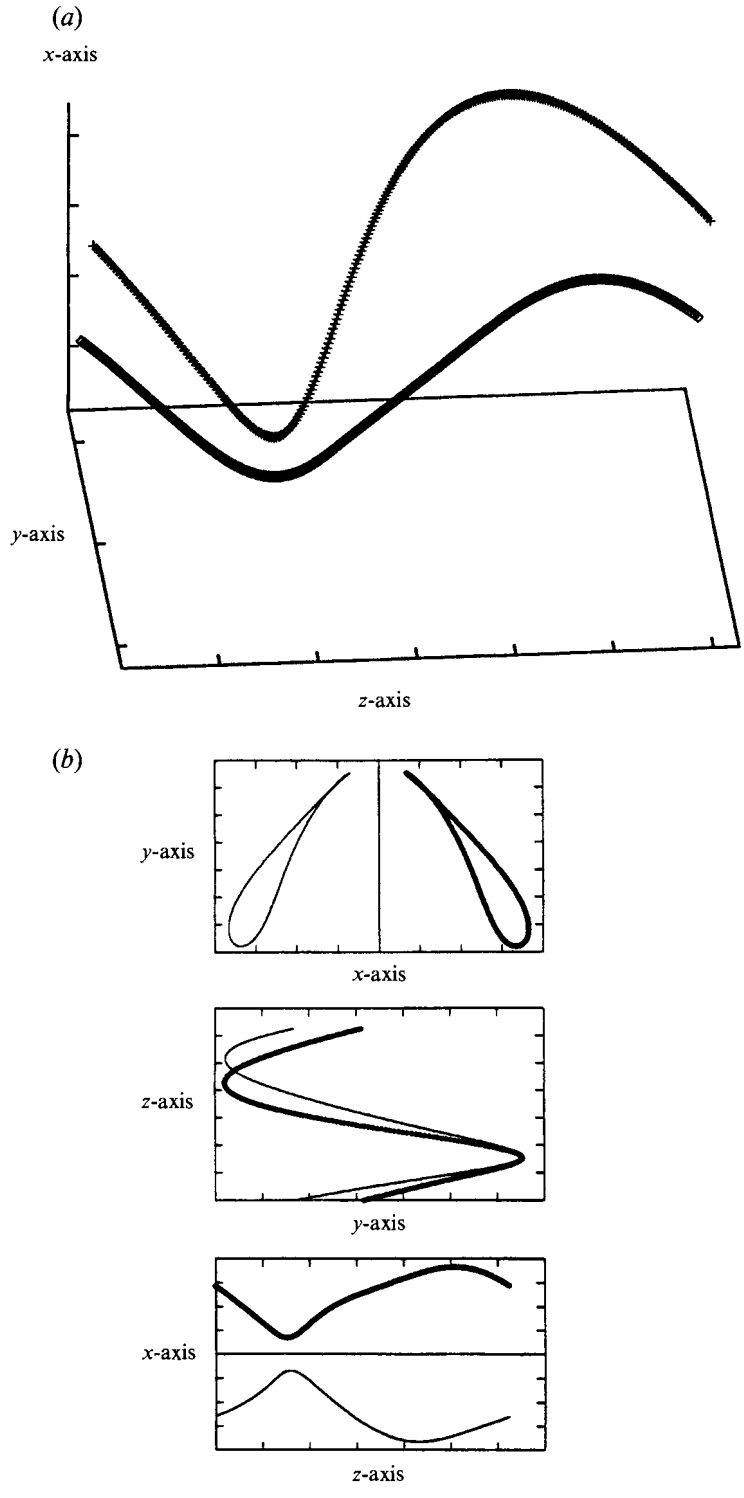

FIGURE 9. Snapshot of filaments for antisymmetric perturbation and $\Gamma = -1$ at time $t = 0.28$.

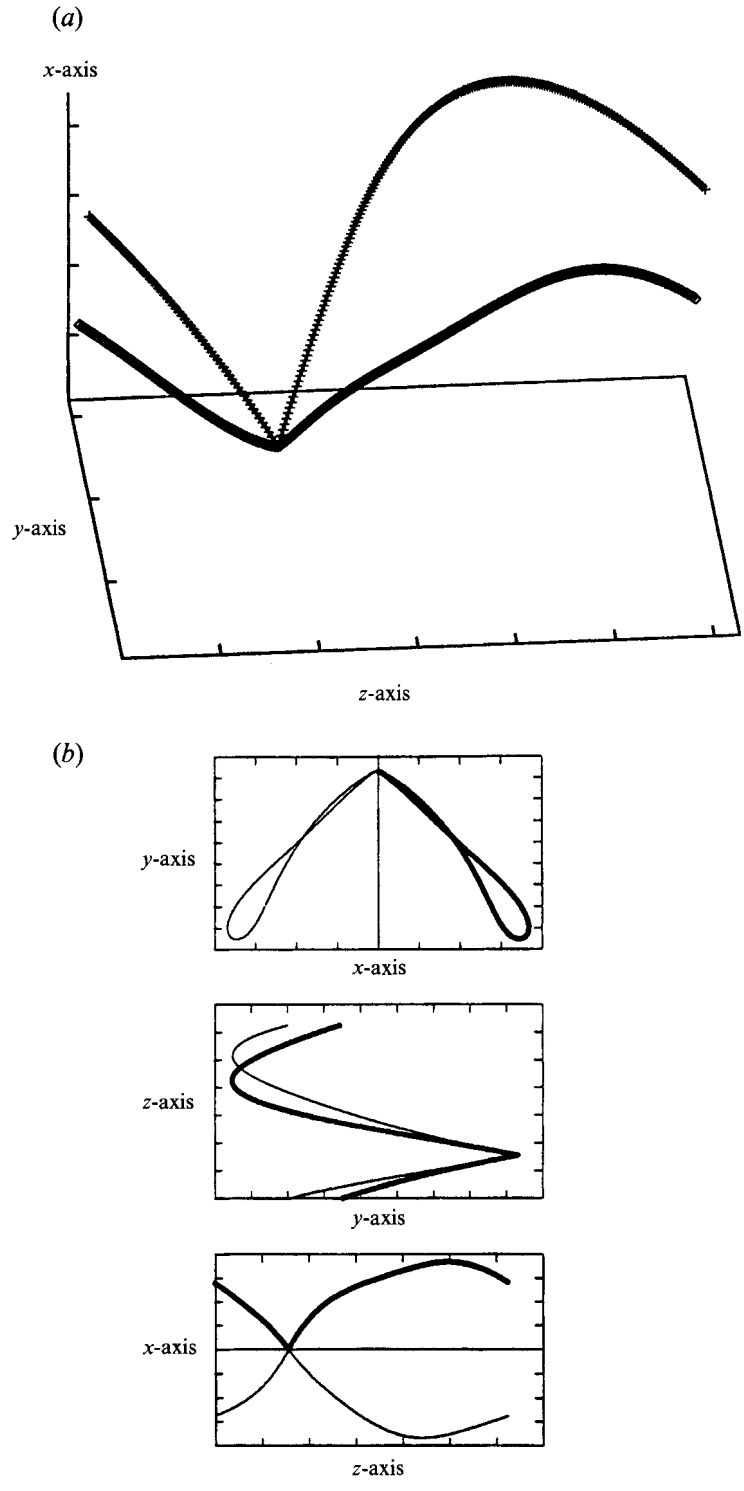

FIGURE 10. Snapshot of filaments for antisymmetric perturbation and $\Gamma = -1$ at time $t = 0.7068$.

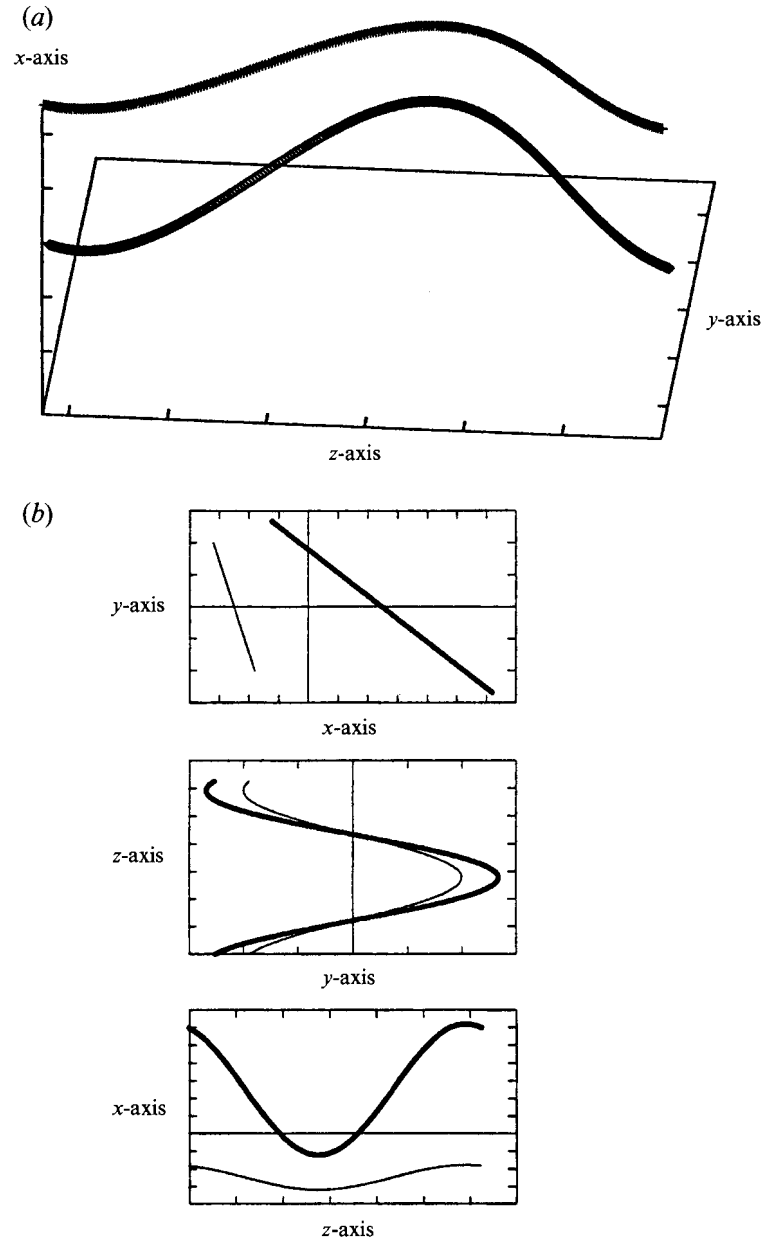

FIGURE 11. Snapshot of filaments for the large-amplitude perturbation from (5.2) and $\Gamma = -0.5$ at time $t = 0$.

always evolve toward a specific symmetric nonlinear solution describing finite-time collapse. Such similarity solutions are discussed at the end of this section. The authors (Damodaran 1994) have tested the nonlinear behaviour of solutions of the filament equations for $\Gamma = -1$ with four other distinct types of initial filament configurations and all of these cases eventually evolve locally to a universal symmetric nonlinear collapse as described in figures 6 and 7; lack of space prevents a detailed description of these additional results here.

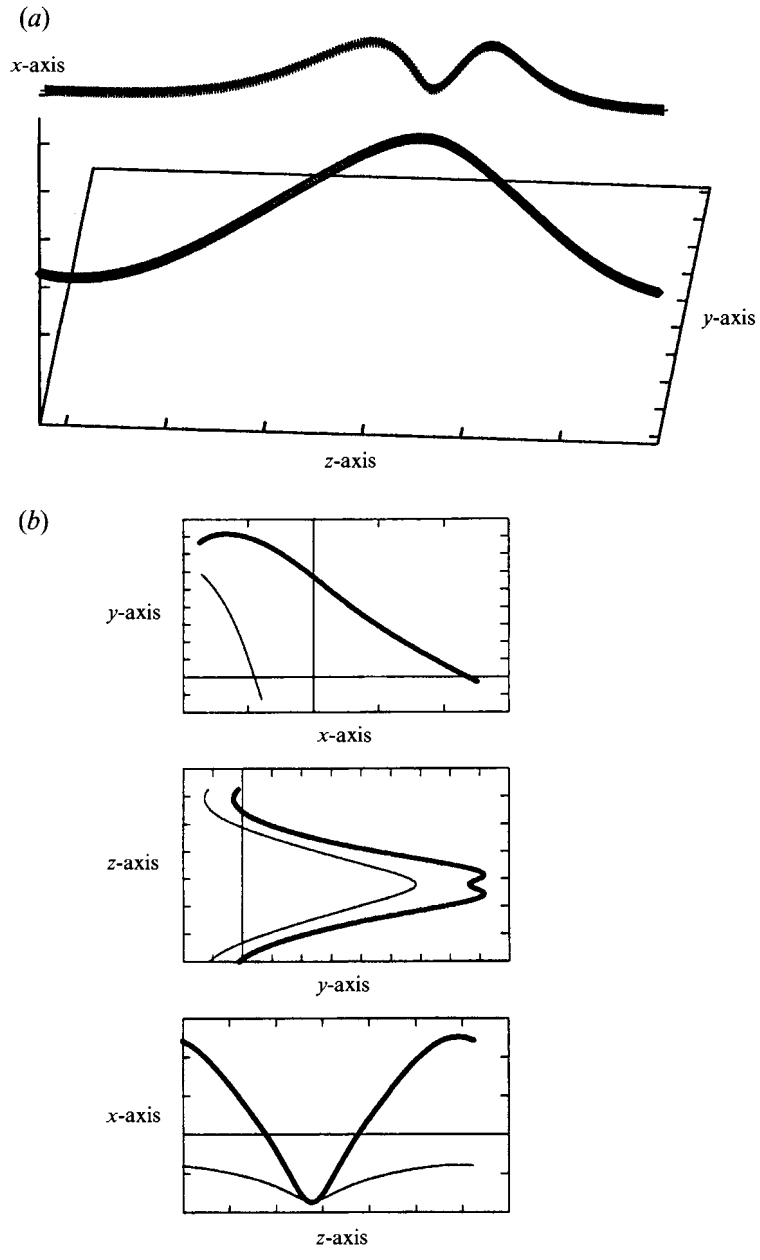

FIGURE 12. Snapshot of filaments for the large-amplitude perturbation from (5.2) and $\Gamma = -0.5$ at time $t = 0.1500$.

Nonlinear collapse for $\Gamma = -0.5$

Here we present evidence for universal behaviour in the local nonlinear collapse of solutions with $\Gamma = -0.5$; however, the universal structure for this collapse depends in an interesting fashion on Γ for these negative circulation ratios. First we consider the solution of the filament equations in (4.2) for $\Gamma = -0.5$ with initial data with the form given in (5.2) with the larger amplitude, A, adjusted so that the minimum separation distance initially is 0.4. The nonlinear solution exhibits finite-time collapse at

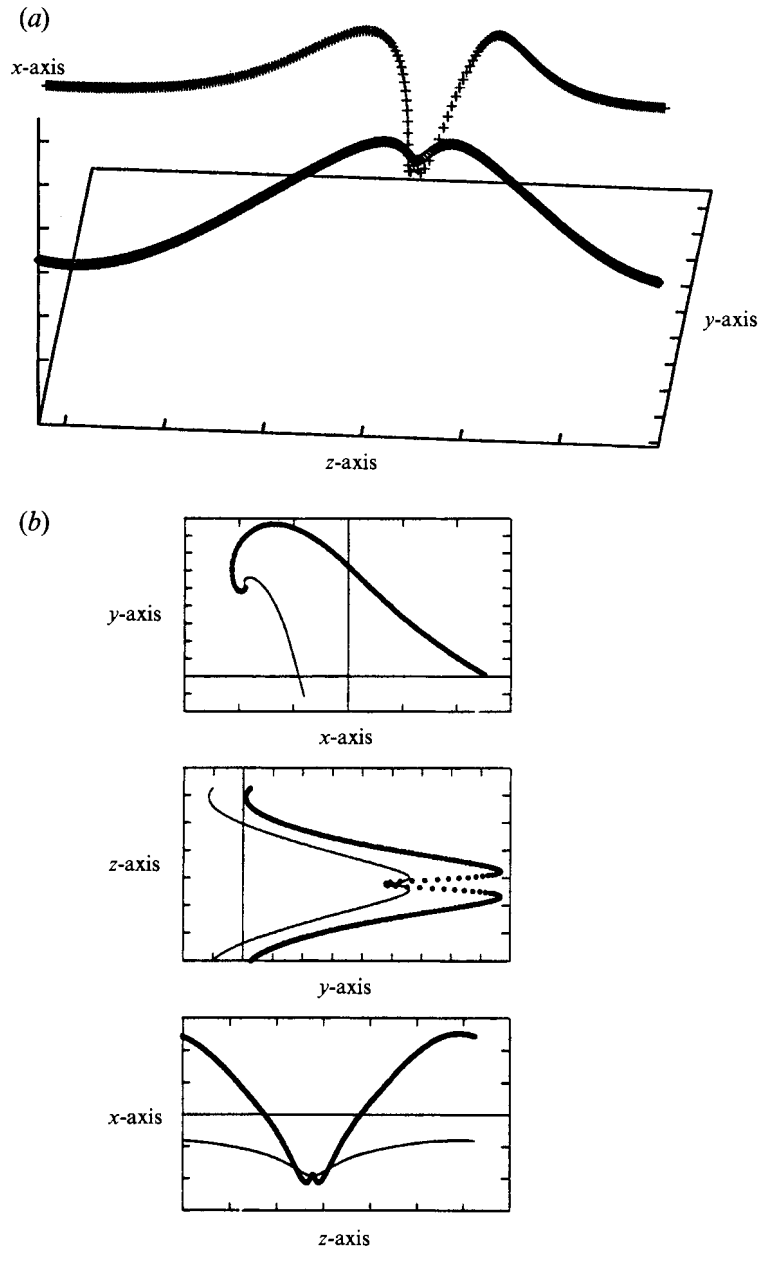

FIGURE 13. Snapshot of filaments for the large-amplitude perturbation from (5.2) and $\Gamma = -0.5$ at time $t = 0.1735$.

$t = 0.1735$ and the time history of the minimum separation distance, $d_*(t)$, has a monotone character qualitatively resembling that from figure 4(*b*). Snapshots of the evolving solution at the times $t = 0$, 0.1500 and 0.1735 are presented in figures 11, 12 and 13, respectively. An important qualitative feature is that there is much more local rotation without spatial translation in this situation with $\Gamma = -0.5$ as compared to the earlier case with $\Gamma = -1$ where translation dominates; this is easy to understand with the rotating motion of point vortices in (4.15) for $\Gamma \neq -1$. As depicted in figures 12 and 13, this local rotation gives a qualitatively different structure for the local collapse for

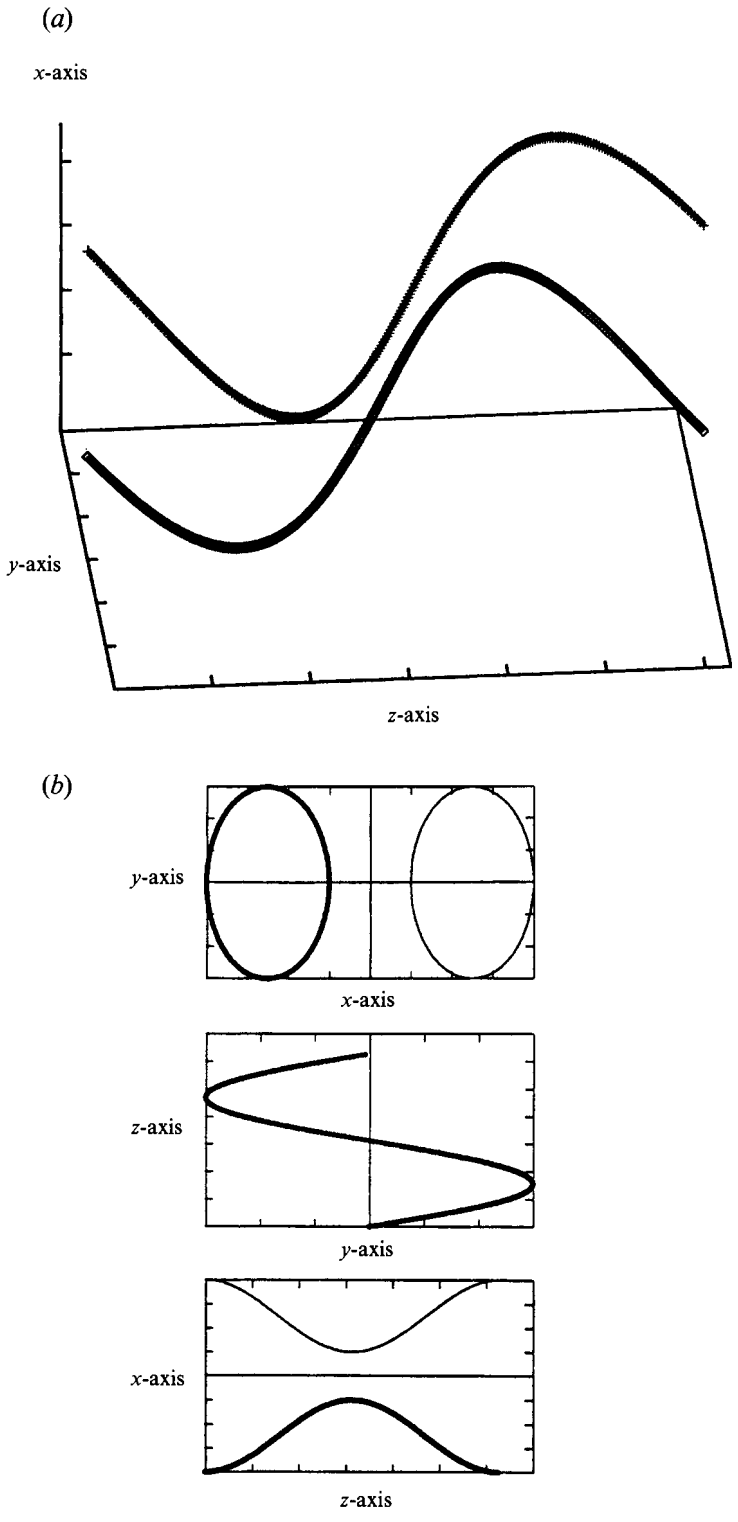

FIGURE 14. Snapshot of the solution for symmetric perturbations and $\Gamma = -0.5$ at $t = 0$.

$\Gamma = -0.5$ which occurs when the filament with smaller circulation loops around the filament with larger circulation and is sucked in by it. This process is shown clearly by the coordinate projections in figures 12(*b*) and 13(*b*).

To demonstrate that a similar local structure for the finite-time collapse occurs with different initial data, we consider the solution of the filament equations with $\Gamma = -0.5$ but with symmetric helical initial perturbations of the filament pair with the form

$$\left.\begin{aligned} \psi_1 &= -0.5 - 0.3\,\mathrm{e}^{-\mathrm{i}\sigma}, \\ \psi_2 &= 0.5 + 0.3\,\mathrm{e}^{-\mathrm{i}\sigma}. \end{aligned}\right\} \tag{5.4}$$

The solution exhibits wave collapse at the time $t = 0.2305$ and snapshots of the filament curves for the times $t = 0$, 0.2000 and 0.2305 are presented in figures 14, 15 and 16, respectively. It is clearly evident by comparing figures 15 and 16 with 12 and 13 that the local nature of the finite-time collapse with this second initial data is essentially the same as that presented in the early case. Furthermore, other systematic studies (Damodaran 1994) with four different types of initial data yield the same local nonlinear structure for collapse with $\Gamma = -0.5$ as presented here. All of these calculations support the notion discussed at the end of this section that there is a universal self-similar form for the collapse for any negative circulation ratio with a structure which varies in an interesting fashion with Γ.

5.2. *Nonlinear waves without collapse for positive circulation ratios*

The elementary analysis from §4 suggests very different behaviour of solutions of the filament equations in (4.2) for positive circulation ratios, $\Gamma > 0$, in contrast to the behaviour just documented in §5.1 for $\Gamma < 0$. In particular the analysis in §5.1 for $\Gamma = 1$ yields the complete nonlinear decoupling of symmetric and antisymmetric modes in (4.7) with exact wavelike solutions. Furthermore, the linearized stability analysis for vortex filament pairs from §4.3 yields a prediction of neutral stability and wavelike behaviour for any positive circulation ratio, Γ, in contrast to the situation with $\Gamma < 0$.

The authors have studied the nonlinear evolution of solutions of the filament equations with ten different types of initial data for the representative positive circulation ratios with $\Gamma = 1$ and $\Gamma = 0.5$. The initial filament geometry, the initial minimum separation distance, and the smallest minimum separation distance over the time interval $t = 0$ to $t = 2$ for each of the ten cases are summarized in table 1.

As the data in table 1 indicate, no finite-time collapse occurs and for eight of the numerical experiments the smallest minimum separation distance over this time interval is comparable in magnitude to the initial separation distance. In two special cases for $\Gamma = 1$ and $\Gamma = 0.5$, respectively, by utilizing very special initial filament structures involving plane curves in orthogonal planes, the authors were able to document cases where the smallest minimum separation distance is nearly an order of magnitude smaller than the initial minimum separation distance. Furthermore, in all ten cases, the solutions of the filament equations exhibited nonlinear wavelike behaviour as predicted by the elementary analysis in §§4.1 and 4.3.

We illustrate this typical wavelike behaviour through the snapshots of the solution in figure 17 for the case in table 1 with $\Gamma = 1$ and the smallest minimum separation distance as time evolves. For this case, the initial data for the two filaments involves two plane curves in orthogonal planes with filament functions initially given by

$$\left.\begin{aligned} \psi_1 &= -0.5 - 0.3\cos\sigma, \\ \psi_2 &= 0.3\mathrm{i}\sin\sigma. \end{aligned}\right\} \tag{5.5}$$

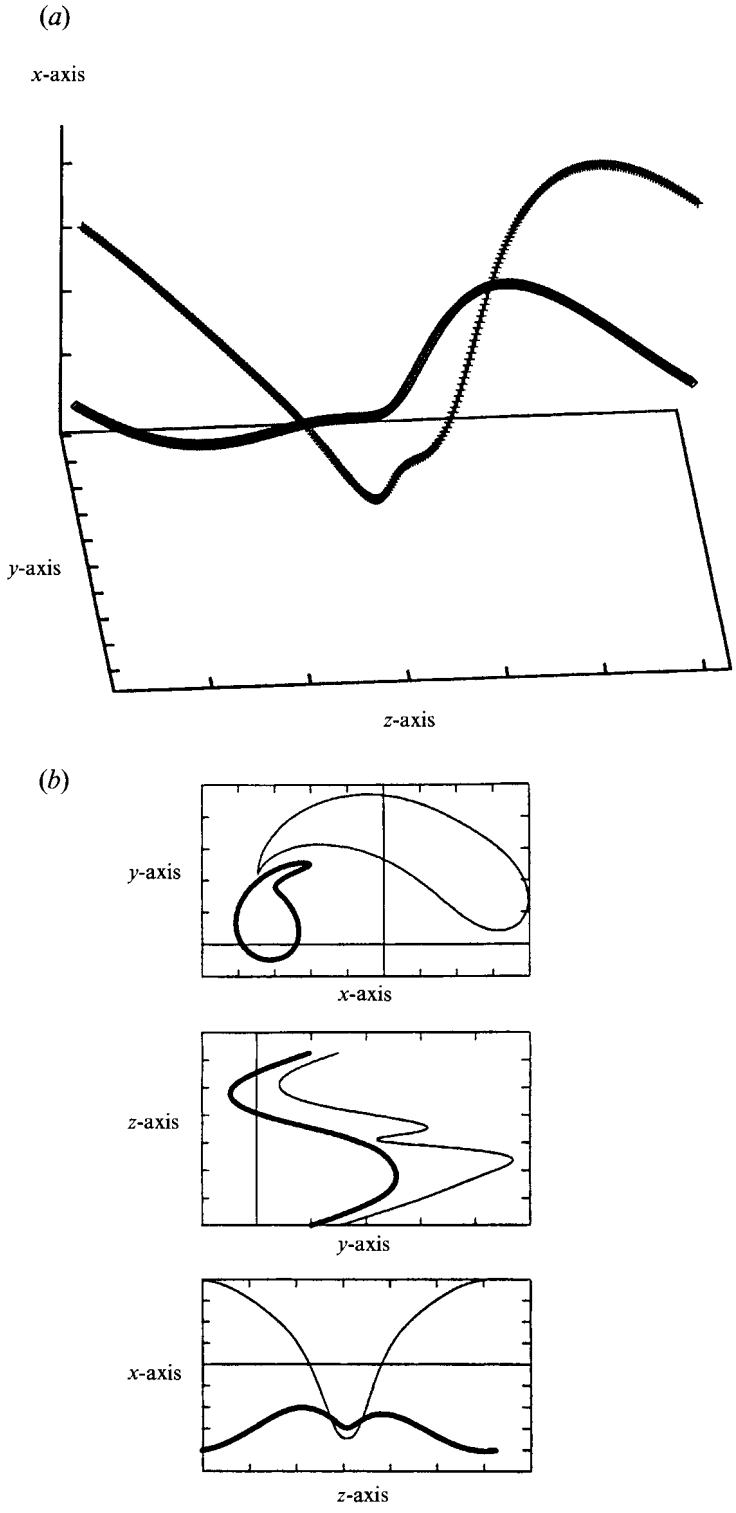

FIGURE 15. Snapshot of the solution for symmetric perturbations and $\Gamma = -0.5$ at $t = 0.2000$.

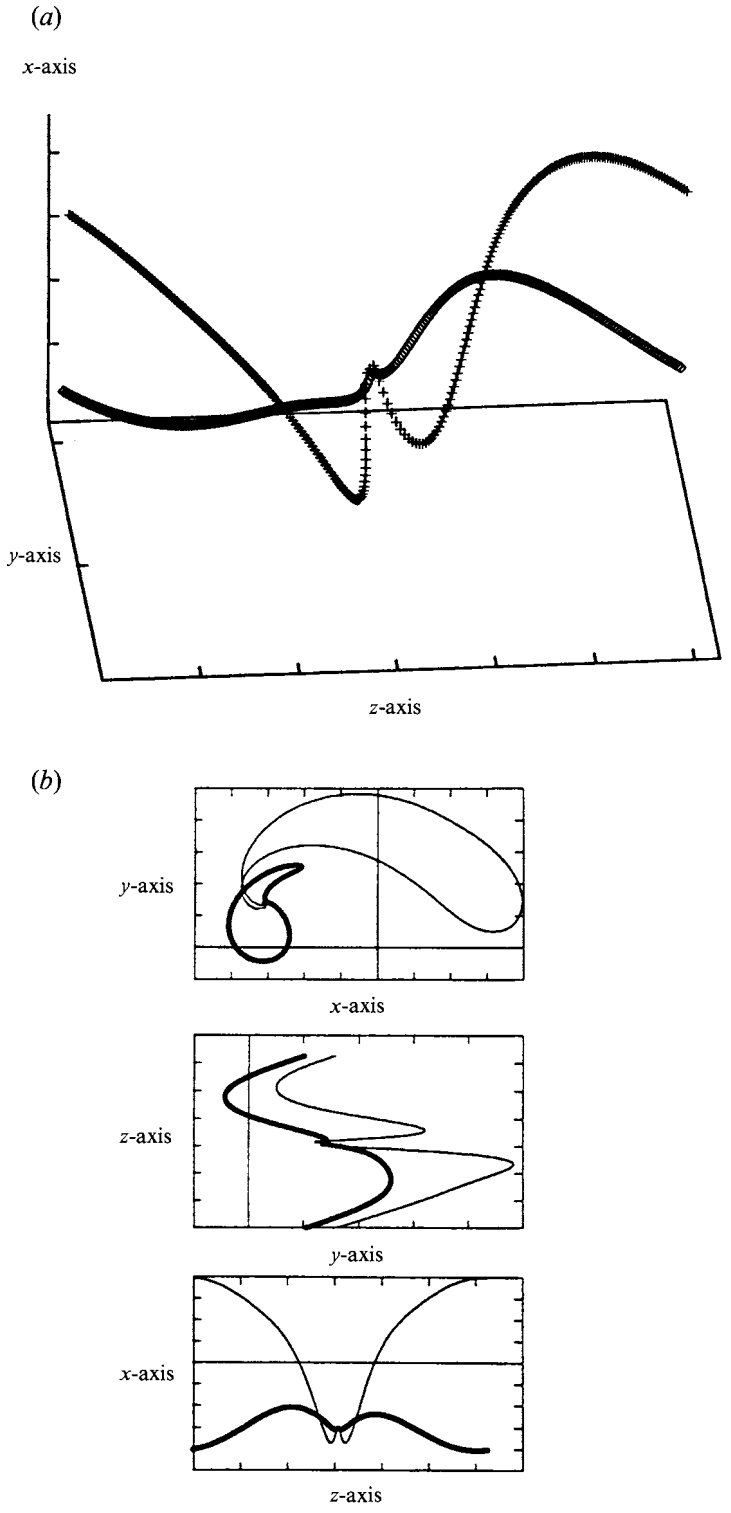

FIGURE 16. Snapshot of the solution for symmetric perturbations and $\Gamma = -0.5$ at $t = 0.2305$.

Circulation ratio	Initial geometry	Initial minimum distance	Smallest minimum distance
$\Gamma = 1$	Symmetric perturbations, helical curves	0.4	0.26
	Antisymmetric perturbations, helical curves	1	1
	Antisymmetric perturbations, plane curves (same plane)	1	1
	Multi-mode data†	0.4	0.25
$\Gamma = 0.5$	Symmetric perturbations, helical curves	0.4	0.27
	Symmetric perturbations, plane curves	0.4	0.28
	Antisymmetric perturbations, helical curves	1	0.83
	Antisymmetric perturbations, plane curves (same plane)	1	0.87
$\Gamma = 1$	Plane curves in orthogonal planes	0.2	0.037
$\Gamma = 0.5$	Plane curves in orthogonal planes	0.2	0.035

† The multi-mode data considered were $\psi_1 = -0.5-0.3\exp(-\sigma)+0.25\exp(2i\sigma)$ and $\psi_2 = 0.5+0.3\exp(i\sigma)+0.25\exp(2i\sigma)$; in all other cases, the initial data involves only the largest wavelength 2π.

TABLE 1

In figures 17(*a*)–17(*d*) we show the filament curves at the times $t = 0$, 0.3, 0.908 and 0.940, respectively. For graphical display these curves have been shifted π-units. The initial minimum separation distance is 0.2 and $t = 0.908$ is the time with the smallest minimum separation distance with value 0.037. The wavelike evolution of the solution is evident from these figures; furthermore, the solution as presented at the later time $t = 0.940$ in figure 17*d*) clearly passes through the time, $t = 0.908$, with smallest minimum separation distance in a wavelike fashion without exhibiting any tendency toward collapse.

5.3. *Self-similar behaviour for the finite time collapse*

In §5.1, we have presented substantial evidence for the universal local self-similar finite-time collapse of general solutions of the filament pair equations in (4.2) for any negative circulation ratio, $\Gamma < 0$ while the nature of this local collapse exhibits interesting dependence on the circulation ratio. In his note, Zakharov (1988) suggested the possibility of finding special self-similar collapsing solutions of his proposed equations in (4.14) for symmetric perturbations of the anti-parallel pair; furthermore, he suggested the similarity law

$$\left.\begin{aligned} u &= (t-t_0)^{1/2} g(\eta), \\ \eta &= \frac{\sigma}{(t-t_0)^{1/2}}, \end{aligned}\right\} \tag{5.6}$$

for special solutions of (4.14). Next, we consider general self-similar solutions of the filament pair equations in (4.2) for an arbitrary circulation ratio and recover a generalization of the scaling ansatz in (5.6). We remind the reader that the equations

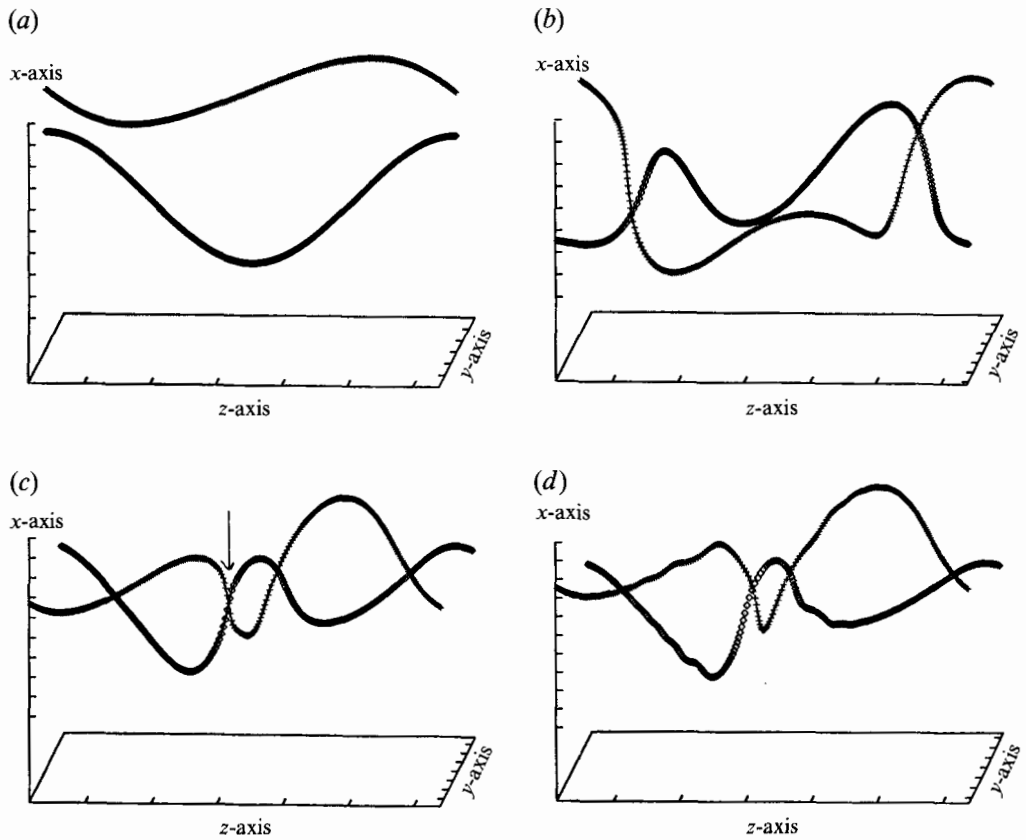

FIGURE 17. Snapshots of the solution with initial data for the filaments involving two plane curves in orthogonal planes at the times (*a*) $t = 0$; (*b*) $t = 0.300$; (*c*) $t = 0.908$, the time with smallest separation distance; (*d*) $t = 0.940$.

which we derived through systematic asymptotic principles in general and in particular, in (4.13) for symmetric perturbations of the anti-parallel pair, do not have the peculiar logarithmic coefficient dependence as proposed by Zakharov (1988) and summarized in (4.14); this will actually simplify the calculations and naturally leads to (5.6) in this special case.

We consider the filament pair equations in the form developed in (4.6), i.e.

$$\left.\begin{aligned} \frac{1}{i}\phi_t &= \tfrac{1}{2}(1+\Gamma)\,\phi_{\sigma\sigma} + \tfrac{1}{2}(1-\Gamma)\left[\psi_{\sigma\sigma} - 4\frac{\psi}{|\psi|^2}\right], \\ \frac{1}{i}\psi_t &= \tfrac{1}{2}(1-\Gamma)\,\phi_{\sigma\sigma} + \tfrac{1}{2}(1+\Gamma)\left[\psi_{\sigma\sigma} + 4\frac{\psi}{|\psi|^2}\right]. \end{aligned}\right\} \tag{5.7}$$

In standard fashion, we seek a symmetry group which leaves the equations in (5.7) invariant. We calculate the stretching transformations

$$\left.\begin{aligned} t' &= \lambda t, \quad & \psi' &= \lambda^c \psi, \\ \sigma' &= \lambda^a \sigma, \quad & \phi' &= \lambda^d \phi, \end{aligned}\right\} \tag{5.8}$$

which leave the equations in (5.7) invariant, and elementary computations show that this is the case for $a = c = d = \frac{1}{2}$. Thus, from general theoretical considerations (Logan

1987) we necessarily seek general similarity solutions of the first kind for the equations in (5.7) with the form

$$\left.\begin{aligned} \eta &= \frac{\sigma}{(t-t_0)^{1/2}}, \\ \phi &= (t-t_0)^{1/2} g(\eta), \\ \psi &= (t-t_0)^{1/2} f(\eta). \end{aligned}\right\} \tag{5.9}$$

By substituting the ansatz from (5.9) into (5.7) we obtain the coupled pair of second-order ordinary differential equations for the two complex-valued functions, $f(\eta), g(\eta)$, given by

$$\left.\begin{aligned} \frac{1}{\mathrm{i}}\eta f' - f &= (1-\Gamma) g'' + (1+\Gamma)\left[f'' + \frac{4f}{|f|^2}\right], \\ \frac{1}{\mathrm{i}}\eta g' - g &= (1+\Gamma) g'' + (1-\Gamma)\left[f'' - \frac{4f}{|f|^2}\right]. \end{aligned}\right\} \tag{5.10}$$

With the formulae in (5.9) and (5.10), which we have developed here, we have both recovered and generalized for the filament pair equations in (4.2) Zakharov's proposed similarity law from (5.6) for the equation in (4.14) with peculiar logarithmic factors.

Obviously, it is an extremely interesting mathematical issue to study the existence and structure of the solutions of (5.10) as a function of the circulation ratio, Γ. The numerical evidence presented earlier in this section leads us to conjecture that such similarity solutions with suitable boundary conditions at infinity exist for the negative circulation ratios, $\Gamma < 0$. Such solutions probably do not exist for positive circulation ratios, $\Gamma > 0$, although it is possible that similarity solutions do exist in this case but are dynamically unstable. Use of the conserved quantities from §3 and listed in (4.3) combined with suitable boundary conditions at infinity should be useful in reducing the degrees of freedom for the two complex ordinary differential equations in (5.10).

Here, we make a more modest contribution and simply check the validity of the proposed self-similar scaling behaviour near the time of collapse for two representative numerical solutions computed in §5.1 for the circulation ratios, $\Gamma = -1, -0.5$. According to the scaling laws predicted in (5.9), the minimum separation functional, $d_*(t)$, should approximately satisfy the scaling relation

$$\log d_*(t) = -\tfrac{1}{2}\log\left(\frac{1}{(T_*-t)}\right), \tag{5.11}$$

where T_* is the finite collapse time. In figure 18, we give log–log plots of the computed minimum separation distance for solutions of (4.2) versus the straight line predicted from (5.11). In figure 18(*a*) we use the solution for $\Gamma = -1$ with the initial data in (5.1) and depicted in figures 5–7 while in figure 18(*b*) we use the solution for $\Gamma = -0.5$ with the initial data in (5.4) and depicted in figures 14–16. For the case with $\Gamma = -1$ in figure 18(*a*), the behaviour in (5.11) is confirmed for a wide range of scales extending to several decades including surprisingly small distances from the collapse time where the detailed numerical resolution is questionable. For the case with $\Gamma = -0.5$, the fit between the computations and the predicted scaling is excellent over a somewhat narrower but still significant range and appreciable deviation develops afterwards. This deviation is probably due to inadequate numerical resolution of the finer scale temporal development of the collapse of the filament pairs which is more complicated for $\Gamma = -0.5$ than for $\Gamma = -1$. Nevertheless, these results support the conjectured self-similar scaling behaviour from (5.11).

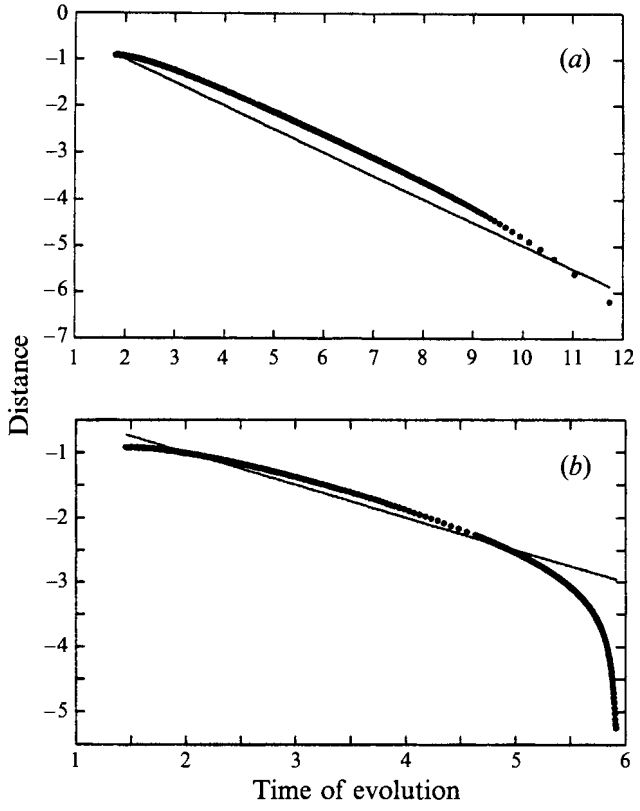

FIGURE 18. Log–log plots of minimum separation distance as a function of time compared with the theoretical prediction of the self-similar scaling law for (*a*) $\Gamma = -1$ and symmetric perturbations and (*b*) $\Gamma = -0.5$ and symmetric helical perturbations.

6. Comparison of vortex interaction theories

In this section we compare existing theories for linear and nonlinear interactions of nearly parallel vortex filaments with the new theory presented in this paper. We first summarize in §6.1 the linear stability theories by Crow (1970) and Jimenez (1975) for antiparallel and parallel vortex pairs and compare with the linearized stability theory for the present asymptotic regime as presented in §4.3. By analysing the long-wave unstable symmetric modes of Crow's explicitly, we will show that our results are consistent with the earlier approaches in that they arise from these through a specific long-wave limit.

As linearly unstable perturbations grow, nonlinear effects become important. In §6.2 we discuss two nonlinear mechanisms of very different nature, namely curvature nonlinearities and the potential vortex interaction. Both mechanisms are potentially relevant for interactions of nearby slender vortices, but they become active in very different regimes for wavelengths and amplitudes of the geometrical vortex filament perturbations. In §6.3 we will discuss the importance of these nonlinear mechanisms for the stability of a vortex pair by contrasting Klein & Majda's (1993) work on the regime with curvature nonlinearity with the present results.

Before we enter the detailed discussion, we summarize the perturbation scaling assumptions that are relevant in the different regimes mentioned above. Common to all of the analyses presented by Crow (1970), Jimenez (1975), Klein & Majda (1993)

and in this paper, is the assumption that the lengthscales and geometrical perturbation amplitudes of the vortex filament displacements are asymptotically large compared to the vortex core sizes δ' (primes denote dimensional quantities in this section). In contrasting the different scalings, it is useful to introduce the unperturbed vortex filament separation distance d' as a reference scale for the characteristic perturbation amplitude A' and perturbation wavelength Λ' in the different regimes. Then these regimes are characterized as follows:

(i) In the Klein–Majda (1993) theory, one has

$$\frac{A'}{d'} = O(\epsilon), \quad \frac{\Lambda'}{d'} = O(1).$$

(ii) In the present paper, we consider perturbations with

$$\frac{A'}{d'} = O(1), \quad \frac{\Lambda'}{d'} = O\left(\frac{1}{\epsilon}\right),$$

where ϵ is a small parameter related to the core size to separation distance ratio via

$$\frac{e^{-1/\epsilon^2}}{\epsilon} = \frac{\delta'}{d'} \ll 1$$

(see §2, equations (2.3) and (2.12)).

(iii) The linearized analyses of Crow (1970) and Jimenez (1975) (and the linearized Klein–Majda results) are valid in both the regimes for Λ'/d' from (i) and (ii), provided that infinitesimal amplitudes are considered, i.e. the limit $A' \to 0$.

We will support the last statement in §6.1 and discuss the crucially different nonlinear effects in the regimes from (i) and (ii) in §§6.2 and 6.3.

6.1. *Linear stability of parallel vortex pairs*

Crow (1970) and Jimenez (1975) studied the linear stability of pairs of counter-rotating and corotating nearly parallel slender vortices of equal strength, respectively. Even though they used an *ad hoc* regularization of the singular line-Biot-Savart integrals for the two vortices, they were able to identify the key stability features of these vortex configurations for infinitesimal disturbances. In particular, linearized non-local vortex–vortex interactions and vortex self-interactions through the Biot-Savart integrals were properly accounted for and the mutual potential vortex interaction, responsible for two-dimensional point-vortex dynamics in the limit of exactly straight parallel vortices, appears in a small-displacement linearization.

The linearized dynamics of a pair of nearly straight vortex filaments with arbitrary relative strengths can be cast into the form

$$\left.\begin{aligned} \frac{1}{\mathrm{i}}\tilde{\psi}_{1,\tau} &= \tilde{\psi}_{1,\sigma\sigma} + \epsilon^2\left[-\mathscr{I}[\tilde{\psi}_1] - \frac{2}{d}((1+\Gamma)\tilde{\psi}_1 + \Gamma\bar{\tilde{\psi}}_1)\right] - \epsilon^2\Gamma[\mathscr{I}^d[\tilde{\psi}_2] - \mathscr{M}^d[\mathrm{Re}\,\tilde{\psi}_2]] \\ \frac{1}{\mathrm{i}}\tilde{\psi}_{2,\tau} &= \Gamma\tilde{\psi}_{2,\sigma\sigma} + \epsilon^2\left[-\Gamma\mathscr{I}[\tilde{\psi}_2] - \frac{2}{d}((\Gamma+1)\tilde{\psi}_2 + \bar{\tilde{\psi}}_2)\right] - \epsilon^2[\mathscr{I}^d[\tilde{\psi}_1] - \mathscr{M}^d[\mathrm{Re}\,\tilde{\psi}_1]], \end{aligned}\right\} \tag{6.1}$$

(see Klein & Majda 1993; Klein 1994). Here $\tilde{\psi}_2(\sigma,\tau), \tilde{\psi}_1(\sigma,\tau)$ are complex functions, whose real and imaginary parts are the components of the displacement vectors $\boldsymbol{X}^{(2)}_{1,2}$ in and normal to the plane spanned by the unperturbed filaments, respectively. Notice that the definition is with respect to the frame of reference defined by the unperturbed straight filaments, which rotate around each other at a constant frequency if $\Gamma \neq -1$.

Thus the definition slightly differs from that of ψ_1, ψ_2 in (4.1). The variable $\sigma = s'/d'$ is a dimensionless straight line coordinate on the unperturbed filament axes in accordance with the scaling assumptions under (i) above.

The symbol $\mathscr{I}[\cdot]$ in (6.1) denotes the self-induction operator from (2.7), d is the non-dimensional leading-order unperturbed filament separation and $\mathscr{I}^d[\cdot], \mathscr{M}^d[\cdot]$ are the linearized coupling operators

$$\left.\begin{aligned} \mathscr{I}^d[w](\sigma) &= \int_{-\infty}^{\infty} \frac{w(\sigma+h) - hw'(\sigma+h)}{(h^2+d^2)^{3/2}}\,\mathrm{d}h, \\ \mathscr{M}^d[w](\sigma) &= \int_{-\infty}^{\infty} \frac{3d^2 w(\sigma+h)}{(h^2+d^2)^{5/2}}\,\mathrm{d}h, \end{aligned}\right\} \tag{6.2}$$

whose features have been discussed in detail by Klein & Majda (1993). In the equations from (6.1) we have correctly accounted for the global rotation of the vortices about their centre of vorticity in the planes normal to the unperturbed axes through the terms involving $(1+\Gamma)$. These terms have erroneously been ignored in the earlier publication by Klein & Majda (1993). (Notice, however, that all their numerical evaluations of the asymptotic equations were for $\Gamma = -1$, where there is no rotation, so that the main results in that work are not affected.)

The equations in (6.1) are valid for any value of $\Gamma = O(1)$. Thus, they are equivalent to Crow's (1970) linearized perturbation equations for $\Gamma = -1$, and they yield Jimenez' (1975) linearized dynamics for corotating vortices for $\Gamma = +1$. Jimenez finds neutral stability for the corotating pair at all wavelengths in agreement with our results in §4.3. Crow's analysis predicts neutral stability of a counter-rotating pair only for perturbation wavelengths comparable to the unperturbed filament separation. He shows that antisymmetric modes (see the definition in (4.12)) are neutrally stable for all wavelengths, but that two bands of instability for symmetric modes exist. There is a long-wave instability at wavelengths of order $O(d'/\epsilon)$ and a short-wave unstable band for wavelengths of order $O(\delta d'/\epsilon)$, with δ from (2.12) (see Klein & Majda (1993) for a detailed discussion of Crow's results regarding their ϵ-dependence).

The first band, $O(d'/\epsilon)$, involves perturbation wavelengths large compared to the unperturbed filament separation. It is these long-wave instabilities that lead to large-amplitude displacements and final merging of trailing vortices behind an aircraft as depicted in figure 1 of Crow (1970). The high-wavenumber band is associated with deformations on the lengthscale of the vortex core diameter. Since the perturbation theories cited rely on the assumption that any geometrical distortion of a vortex must have a characteristic length large compared to the vortex core size, this high-wavenumber band must be dismissed as spurious. A modified theory that does not use the slender vortex approximation and considers distortions of the vortex core structure is necessary to consistently describe instabilities in this high-wavenumber range (see Widnall (1975) and the references therein). We remark, however, that the nonlinear generation of short-wave solution components from long-wave initial data as observed by Klein & Majda (1991*a*, 1993) in the framework of the slender vortex filament theory is not at all a spurious process.

We recall from (2.3) that the nonlinear theory presented in this paper is valid for geometrical perturbations of the vortex filaments with wavelengths large compared to the unperturbed separation distance: We consider wavelength of order $O(\epsilon R') = O(d'/\epsilon)$, while the displacements and the unperturbed separation distance are $O(\epsilon^2 R') = O(d')$, where R' is a typical filament radius of curvature. Considering the discussion of Crow's results for long-wave instabilities, it seems natural to investigate

whether the linearized version of our present theory agrees with the long-wave limit versions of Crow's (1970) or Klein & Majda's (1993) predictions associated with the equations in (6.1).

We intend to compare the wavenumber dependence of the growth rate in the long-wave unstable band for symmetric modes of a counter-rotating pair. Thus we consider the stability results from §4, equations (4.22) and (4.23) for

$$\Gamma = -1 \quad \text{hence} \quad \begin{matrix} a = 0, \\ b = 2. \end{matrix} \tag{6.3}$$

Then we find

$$\mathscr{R} = 4\xi^2, \quad \mathscr{P} = \frac{64\xi^4}{d^4}, \tag{6.4}$$

and

$$\lambda_+^2 = \frac{1}{d^2}(d\xi)^2(4-(d\xi)^2)^{1/2}. \tag{6.5}$$

Next we analyse Crow's or Klein & Majda's formulae for wavenumbers of order $O(\epsilon)$ in their non-dimensional representation. Let k denote the wavenumber variable from Klein & Majda (1993), then the growth function for symmetric modes of the anti-parallel pair consistent with (6.1) is given by

$$\lambda_{Crow} = \operatorname{sgn}(\tilde{p})\tilde{p}^{1/2} \tag{6.6}$$

where

$$\tilde{p}(k) = \frac{2\epsilon^2}{d^2}[(1-\psi+\beta^2\omega)(1+\chi-\beta^2\omega)]^{1/2}, \tag{6.7}$$

with

$$\left.\begin{aligned} \beta &= dk, \\ \omega &= \frac{1}{2\epsilon^2}[1-\epsilon^2(\tfrac{1}{2}\ln k^2 - c_0)], \\ \chi &= \beta K_1(\beta), \\ \psi &= \beta^2 K_0(\beta) + \beta K_1(\beta). \end{aligned}\right\} \tag{6.8}$$

Here K_0, K_1 are the modified Bessel functions of zeroth and first-order and c_0 is a constant.

To compare (6.6)–(6.8) with (6.3)–(6.5) we notice that wavelengths that are by a factor of $1/\epsilon$ larger than the unperturbed filament separation distance correspond to wavenumbers $k = O(\epsilon)$ in the Klein–Majda theory. Thus, we let $k = \epsilon\xi$ in (6.6)–(6.8) and extract the leading-order terms. Noticing that

$$\left.\begin{aligned} \beta^2\omega &= \tfrac{1}{2}(\mathrm{d}\xi)^2, \\ \beta^2 K_0(\beta) &= O(\epsilon^2), \\ \beta K_1(\beta) &= 1 + O(\epsilon), \end{aligned}\right\} \tag{6.9}$$

we find the leading-order expression for $\tilde{p}$ from (6.7) as

$$\lambda_{Crow}|_{k=\epsilon\xi} = \frac{\epsilon^2}{d^2}(d\xi)^2(4-(d\xi)^2)^{1/2}(1+O(\epsilon)). \tag{6.10}$$

This coincides with the formula for the growth rates for the unstable eigenvalues from the present work as given in (6.5) except for an excess factor of ϵ^2 in (6.10). This factor is due to the fact that the vortex pair dynamics in the Klein–Majda (1993) regime is by one order of magnitude in ϵ^2 faster than the vortex interactions in the regime

considered here and that the Klein–Majda theory therefore uses a reference time for non-dimensionalization that is by a factor of ϵ^2 shorter than that used in the present analysis. Thus, a trivial time rescaling yields the desired coincidence of the stability results and we conclude that: *The present theory for long-wave, large-amplitude displacements of nearby slender vortex filaments reproduces the linear stability results of Crow (1970) for a counter-rotating vortex pair with equal strengths in the small-wavenumber regime.*

6.2. *Types of nonlinearities relevant for vortex pair stability*

Two-dimensional vortex dynamics

As described in §1, the interaction of point vortices in two dimensions relies on the fact that each member of a collection of point vortices is advected by the sum of the potential vortex velocities induced at its current location by its peers. Therefore, if $\{\boldsymbol{X}_i(t)\}_{i=1}^N$ are the centre locations of the vortices, then

$$\frac{\partial \boldsymbol{X}_i}{\partial t} = \boldsymbol{t}_0 \times \sum_{j \neq i} \frac{\Gamma_j}{2\pi} \frac{\boldsymbol{X}_i - \boldsymbol{X}_j}{|\boldsymbol{X}_i - \boldsymbol{X}_j|^2}, \tag{6.11}$$

where $\boldsymbol{t}_0$ is the unit vector normal to the plane of the vortex motion. As two nearly straight parallel slender vortices approach each other, this mutual induction becomes prominent, once their separation is sufficiently small. Being basically two-dimensional in nature, this potential vortex induction will then interact with the inherently three-dimensional effects of mutual and self-induction owing to geometrical distortions of the filament centrelines. We have analysed this scenario extensively in the earlier sections of this paper.

The local induction approximation and Hasimoto's transform

On the other hand, Arms & Hama (1965) consider the self-induced motion of a single vortex filament in three space dimensions. Neglecting all non-local effects, they formulated the 'local induction approximation', which amounts to the evolution equation

$$\frac{\partial \boldsymbol{X}}{\partial \bar{t}} = \kappa \boldsymbol{b}, \tag{6.12}$$

for the filament centreline $\mathscr{L}(\bar{t})\colon s \to \boldsymbol{X}(s, \bar{t})$. Here $\bar{t} = \Gamma t / 4\pi\alpha\epsilon^2$ (see (2.14) for the definition of α) is a suitably scaled time variable, κ is the local curvature of the filament centreline and $\boldsymbol{b}$ the local binormal unit vector. Comparison with (2.5) shows that this dynamic equation is a leading-order approximation for the motion of an isolated three-dimensional-vortex filament, provided one is willing to neglect terms of order $\epsilon^2 = \ln^{-1}(1/\delta)$. Hasimoto (1972) introduced a nonlinear transformation in order to simplify the mathematical description of the vortex centreline evolution. He combined information on curvature κ and torsion T of the filament centreline in the complex filament function

$$\psi(s, \bar{t}) = \kappa(s, \bar{t}) \exp\left(\mathrm{i} \int_{s_0}^{s} T(s', \bar{t})\, \mathrm{d}s'\right). \tag{6.13}$$

He was able to identify the three-dimensional-vortex evolution equation (6.12) with the cubic nonlinear Schrödinger equation

$$\frac{1}{\mathrm{i}} \psi_{\bar{t}} = \psi_{\bar{s}\bar{s}} + \tfrac{1}{2}|\psi|^2 \psi, \tag{6.14}$$

for the filament function in (6.13), where $\tilde{s}$ is an arclength coordinate. This work relates in a very clear fashion the local induction dynamics of a vortex with the integrable cubic Schrödinger equation and this allows a complete theoretical classification of curvature-induced nonlinearities of vortex dynamics (Ablowitz & Segur 1981). Hasimoto, for example, shows that the local induction dynamics allows for the formation of solitons on the vortex filament centreline.

This curvature nonlinearity also plays a major role in the self-induction of a single perturbed slender vortex. Klein & Majda (1991*a*, *b*) observe that the local induction approximation of Arms & Hama (1965) and Hasimoto (1972) cannot describe the important mechanism of vortex self-stretching through non-local self-induction (the local induction binormal term does not describe any vortex stretching at all!). Evaluating the general vortex evolution equation from (2.5) for perturbed vortex filaments in the regime from (2.3) and using the Hasimoto transform (6.13), they derive the relevant equation for the time evolution of small-amplitude–short-wavelength perturbations of a nearly straight slender vortex:

$$\frac{1}{\mathrm{i}}\psi_\tau = \psi_{\sigma\sigma} + \epsilon^2(\tfrac{1}{2}|\psi|^2\psi - \mathscr{I}[\psi]). \tag{6.15}$$

Here σ and τ are stretched arclength and time variables as in (2.3) and the $\mathscr{I}[\cdot]$-operator is the one given in (2.7) and (2.8) above. In this regime, the curvature nonlinearity is diminished to first order in ϵ^2, where it has to compete with the linearized non-local contribution from the finite part of the Biot-Savart integral. For a detailed discussion of mathematical features of (6.15) and of the structure of solutions see Klein & Majda (1991*b*).

It turns out that the two very different nonlinear mechanisms from (6.11) and (6.15) both play a role in the evolution of interacting slender vortices, but that they each become dominant in different regimes from the perturbation scalings.

6.3. *Nonlinear stability theories for a vortex pair*

An interaction of non-local induction effects and the cubic curvature nonlinearity was observed by Klein & Majda (1993) in a nonlinear stability analysis of (anti-) parallel pairs of vortex filaments in the regime of perturbation scales stated in (i) at the beginning of this section. This work is a systematic generalization of Crow's linearized (1970) theory in that it (*a*) is based on systematic matched asymptotic expansions for the Navier–Stokes equations and (*b*) allows for perturbation amplitudes that are sufficiently larger to make the Hasimoto-type curvature nonlinearities as important as the non-local induction (just as in (6.15)). The resulting coupled filament equations for a counter-rotating pair including dominant linear curvature effects and an ϵ^2-perturbation with both curvature nonlinearities and non-local induction effects read

$$\left.\begin{aligned}
\frac{1}{\mathrm{i}}\psi_\tau &= (1-\epsilon^2 l^\psi)\,\psi_{\sigma\sigma} + \epsilon^2\left(\tfrac{1}{2}|\psi|^2\psi - \mathscr{I}[\psi] + \frac{2}{d}\bar{\psi}\right) + \epsilon^2(\mathscr{I}^d[\phi] + \mathscr{M}^d[\mathrm{Re}\,\phi]),\\
-\frac{1}{\mathrm{i}}\phi_\tau &= (1-\epsilon^2 l^\phi)\,\phi_{\sigma\sigma} + \epsilon^2\left(\tfrac{1}{2}|\phi|^2\phi - \mathscr{I}[\phi] + \frac{2}{d}\bar{\phi}\right) + \epsilon^2(\mathscr{I}^d[\psi] + \mathscr{M}^d[\mathrm{Re}\,\psi]),
\end{aligned}\right\} \tag{6.16}$$

where ϕ and ψ are Hasimoto-type filament functions for the two vortices defined in analogy with (6.13). The factors $(1-\epsilon^2 l^{\psi,\phi})$ multiplying the dominant linear curvature terms are symmetry breaking arclength corrections, which arise for solutions that have infinite support or that are periodic in σ. Otherwise, (6.16) is equivalent to the

linearized system from (6.1) for $\Gamma = -1$ and with the weak cubic curvature nonlinearities and the arclength corrections supplemented.

It is extremely important to realize precisely the regime of perturbation scales for the vortex filament centrelines in which the equations in (6.16) are valid and to contrast them with the regime considered in this paper. We reiterate that (6.16) is valid for

> displacements of the vortices from their unperturbed positions that are small compared to the unperturbed separation distance d' and for
>
> characteristic perturbation wavelength of the same order as d'.

As a consequence of the first statement, the mutual induction due to the vortices' outer potential flow fields appears in a linearized fashion through the terms multiplied by $2/b$ in (6.16). As a consequence of the second, long-wave perturbations with wavelengths large compared to the filament separation are formally inaccessible in this theory.

This theory of Klein & Majda (1993) is able to explain the nonlinear generation of small scales and local breakdown of vortices through the formation of kinks and hairpin structures. These phenomena arise from the interaction of the curvature nonlinearities with the non-local induction terms at the first order in ϵ^2 as has been shown in other contexts also by Klein & Majda (1991*b*) and Klein *et al.* (1992). However, the linear stability results discussed above raise an important question regarding the nonlinear effects that should become important when the long-wave unstable modes grow to sufficiently large amplitudes. By construction, the theory is designed to describe geometrical perturbations with wavelengths comparable to the unperturbed filament separation distance d'. These wavelengths correspond to wavenumbers of order $O(1)$ under the scalings chosen for (6.16). However, the linear analysis predicts instabilities for perturbations with wavenumbers of order $O(\epsilon)$, corresponding to wavelengths large compared to the unperturbed separation. Now consider a perturbation with wavelength of order d'/ϵ that has grown to produce order one curvature, i.e. $|\psi| = O(1)$. This perturbation will be associated with displacements comparable to d' and larger, so that the linearization $(2/d)\bar{\psi}$ in $(6.16)_1$, say, for the potential vortex interaction is no longer acceptable.

A modified theory is necessary to consistently describe this regime, and the present paper approaches this challenge using systematic perturbation analysis in line with the earlier work of two of the authors. In this regime the potential vortex interaction dominates the curvature nonlinearity and the non-local induction terms and assumes the nonlinear structure explained in (1.4) or (6.11). Importantly, in the regime considered in this paper, the potential vortex interaction occurs at leading order where it then competes directly with the leading linear curvature terms $\psi_{\sigma\sigma}$ and $\phi_{\sigma\sigma}$. This theory cannot describe the generation of small scales due to nonlinear–non-local self- and mutual-induction, but it is suited to predict the nonlinear mutual attraction and tendency toward collapse of trailing vortices behind an aircraft as observed experimentally (see Crow 1970, figure 1).

7. Concluding remarks

It is interesting to study the properties of the general asymptotic filament equations from (1.2) in situations with more than two vortex filaments which arise naturally in models for trailing wakes, etc. Another interesting direction is to develop similar simplified asymptotic approximations for other physical equations with evolving

nearly parallel filamentary structures as occurs in magneto-hydrodynamics, high temperature superconductivity, superfluids, etc. Applications and generalization in both of these directions are currently being developed by the authors and will be reported elsewhere. The general equations from (1.2) are also appealing for a simplified statistical theory of nearly parallel vortex filaments which is intermediate between two- and three-dimensional statistical theories for vortices (Chorin 1988, 1994).

As regards the vortex filament pair, it would be very interesting to develop rigorous mathematical theorems which necessarily prove that finite-time collapse must occur for negative circulation ratios and cannot occur for positive circulation ratios for appropriate initial data. It is even possible that the equations in (4.2) are a completely integrable Hamiltonian system at least for the special circulation ratio, $\Gamma = 1$ (see §4.2) and this possibility merits further investigation.

The authors thank Richard McLaughlin for many perceptive comments and observations regarding the filament equations in (4.2) which he made during the course of this work. Andrew Majda's research is partially supported by grants NSF DMS-99301094, ONR N00014-89-J-1044.P00003, ARO DAAL03-92-G-0010, DARPA N00014-92-J-1796. Rupert Klein's research is partially supported by the Sonderforschungsbereich SFB 25 of the Deutsche Forschungsgemeinschaft.

Appendix. Derivation including the first order in ϵ^2

We consider N nearly parallel slender vortex filaments as discussed in §2. Here we carry out the Biot-Savart-integrals for the foreign-induced velocity of one filament owing to the vorticities of the others. We include the effects of non-locality for completeness, which have been neglected as higher-order terms throughout the main text.

We begin with the equations of motion (2.5),

$$\frac{\partial \boldsymbol{X}_i}{\partial t} = \frac{\Gamma_i}{4\pi}\left(\ln\frac{1}{\delta} + C_i\right)\kappa \boldsymbol{b}_i + \boldsymbol{Q}_i^f + \sum_{j\neq i} \boldsymbol{Q}_{i/j}^{outer}, \tag{A 1}$$

which one obtains via a matched asymptotic analysis (see Callegari & Ting 1978; Klein & Majda 1991*a*; Klein & Knio 1995). We have quoted in §2, equations (2.5) and (2.6) the explicit formulae for the self-induction terms $(\ln 1/\delta + C_i)\,\kappa \boldsymbol{b}_i + \boldsymbol{Q}_i^f$ for slender vortices with perturbed straight-line geometries as in (2.3) from Klein & Majda (1991*a*). Here we give a detailed derivation of the foreign-induced velocities $\boldsymbol{Q}_{i/j}^{outer}$ including the first order in ϵ^2.

The matched asymptotic analysis for the velocity field of a slender vortex involves separate representations of the velocity distribution in the vortical core of the filament and the outer induced irrotational field. In the matching procedure, the small-distance representation of the outer field is compared with the large radius representation of the core velocity distribution. Here we are interested in the velocity that, say, the jth vortex induces at the location of the ith vortex. Since by assumption the vortex cores do not overlap, while the separation distance of the vortex centrelines is $O(\epsilon^2) \ll 1$ compared to a typical filament radius of curvature, we may immediately use the small distance representation of the outer field of the jth vortex to obtain the desired induction at the location of the ith vortex:

$$\boldsymbol{Q}_{i/j}^{outer} = \frac{\Gamma_j}{4\pi}\left\{\frac{2}{r_{j/i}}\boldsymbol{\theta}_{j/i} + (\kappa \boldsymbol{b})_{j/i}\ln\left(\frac{1}{r_{j/i}}\right) + (\kappa\cos\varphi\boldsymbol{\theta})_{j/i} + \boldsymbol{Q}_{j/i}^f\right\}, \tag{A 2}$$

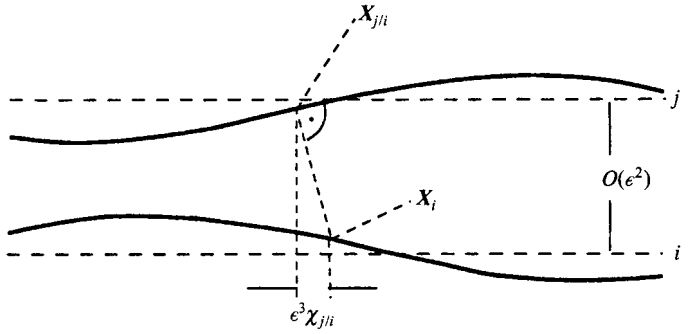

FIGURE 19. Associated points X_i and $X_{j/i}$ on neighbouring filaments.

(see e.g. Ting & Klein 1991). Next we separately provide asymptotic representations of all the terms in (A 2) based on the perturbed curve scalings from (2.3).

First we observe from figure 19 that the two related points X_i and $X_{j/i}$ on the ith and jth vortex are located in nearly the same normal plane to the unperturbed tangent vector t_0:

$$\left.\begin{aligned} X_i &= s_i t_0 + \epsilon^2 X_j^{(2)}\left(\frac{s_i}{\epsilon}, \frac{t}{\epsilon^4}\right) + \ldots, \\ X_{j/i} &= s_{j/i} t_0 + \epsilon^2 X_j^{(2)}\left(\frac{s_{j/i}}{\epsilon}, \frac{t}{\epsilon^4}\right) + \ldots, \end{aligned}\right\} \tag{A 3}$$

where

$$s_{j/i} = s_i + \epsilon^3 \chi_{j/i}^{\epsilon}. \tag{A 4}$$

The scaled axial displacement $\chi_{j/i}^{\epsilon}$, which is graphically explained in figure 19, will be expressed in terms of the perturbation functions $X_i^{(2)}$, $X_j^{(2)}$ and their derivatives below. With these preliminary considerations we can now expand all the terms needed in (A 2).

The distance $r_{j/i} = |X_i - X_{j/i}|$

Using the curve representations in (2.3) we have

$$X_i - X_{j/i} = (s_i - s_{j/i}) t_0 + \epsilon^2 \left\{ X_i^{(2)}\left(\frac{s_i}{\epsilon}, \frac{t}{\epsilon^4}\right) - X_j^{(2)}\left(\frac{s_{j/i}}{\epsilon}, \frac{t}{\epsilon^4}\right) \right\} + O(\epsilon^3). \tag{A 5}$$

Using next (A 4) we may write

$$X_i - X_{j/i} = \epsilon^2 d_e\left(\frac{s_i}{\epsilon}, \frac{t}{\epsilon^4}\right) + \epsilon^3 \chi_{j/i}^{\epsilon} t_0 + \epsilon^4 \chi_{j/i}^{\epsilon} \frac{\partial}{\partial \sigma} X_i^{(2),\epsilon} + \ldots, \tag{A 6}$$

where we have introduced the abbreviations

$$d_e = (X_i^{(2),\epsilon} - X_j^{(2),\epsilon})\left(\frac{s_i}{\epsilon}, \frac{t}{\epsilon^4}\right), \tag{A 7}$$

and

$$X_j^{(2),\epsilon} = \sum_{\nu=2} \epsilon^{\nu-2} X^{(\nu)}, \tag{A 8}$$

and where it is to be understood that $\chi_{j/i}^{\epsilon}$ also has an asymptotic expansion

$$\chi_{j/i}^{\epsilon} = \chi_{j/i}^{(0)}\left(\frac{s}{\epsilon}, \frac{t}{\epsilon^4}\right) + \epsilon \chi_{j/i}^{(1)}\left(\frac{s}{\epsilon}, \frac{t}{\epsilon^4}\right) + \ldots. \tag{A 9}$$

It follows from (A 6) and from the fact that $\boldsymbol{X}_j^{(\nu)} \cdot \boldsymbol{t}_0 \equiv 0$ by assumption (see remark below (2.4)) that

$$|\boldsymbol{X}_i - \boldsymbol{X}_{j/i}|^2 = r_{j/i}^2 = \epsilon^4 \boldsymbol{d}_e^2 + \epsilon^6 \left[(\chi_{j/i}^\epsilon)^2 + 2\chi_{j/i}^\epsilon \boldsymbol{d}_e \cdot \frac{\partial}{\partial \sigma} \boldsymbol{X}_i^{(2),\epsilon} \right] + o(\epsilon^6), \tag{A 10}$$

and thus

$$\frac{1}{r_{j/i}} = \frac{1}{\epsilon^2 d_e} \left(1 - \frac{\epsilon^2}{2 d_e^2} \left[(\chi_{j/i}^\epsilon)^2 + 2\chi_{j/i}^\epsilon \boldsymbol{d}_e \cdot \frac{\partial}{\partial \sigma} \boldsymbol{X}_i^{(2),\epsilon} \right] + \dots \right), \tag{A 11}$$

where $d_e = \boldsymbol{d}_e / |\boldsymbol{d}_e|$. At leading order (A 10) reads

$$r_{j/i} = \epsilon^2 |\boldsymbol{X}_i^{(2)} - \boldsymbol{X}_{j/i}^{(2)}| + O(\epsilon^3). \tag{A 12}$$

The circumferential unit vector $\boldsymbol{\theta}_{j/i}$

The general formula for $\boldsymbol{\theta}_{j/i}$ is

$$\boldsymbol{\theta}_{j/i} = -\frac{\boldsymbol{X}_i - \boldsymbol{X}_{j/i}}{|\boldsymbol{X}_i - \boldsymbol{X}_{j/i}|} \times \boldsymbol{t}_{j/i}, \tag{A 13}$$

where $\boldsymbol{t}_{j/i}$ is the local unit tangent to $\mathscr{L}_j^\epsilon$ in $\boldsymbol{X}_{j/i}$. We have

$$\boldsymbol{t}_{j/i} = \frac{1}{|\partial \boldsymbol{X}_j / \partial s|} \frac{\partial \boldsymbol{X}_j}{\partial s} \left(\frac{s_{j/i}}{\epsilon}, \frac{t}{\epsilon^4} \right). \tag{A 14}$$

Inserting the curve representation from (2.3) we find

$$\boldsymbol{t}_{j/i} = \left(1 - \tfrac{1}{2}\epsilon^2 \left(\frac{\partial}{\partial \sigma} \boldsymbol{X}_j^{(2),\epsilon} \right)^2 + o(\epsilon^2) \right) \left(\boldsymbol{t}_0 + \epsilon \frac{\partial}{\partial \sigma} \boldsymbol{X}_j^{(2),\epsilon} \right), \tag{A 15}$$

where $\sigma = s/\epsilon$. Using the expansion of the distance vector from (A 6) in (A 13) we obtain

$$\boldsymbol{\theta}_{j/i} = \frac{1}{d_e} \left[\boldsymbol{t}_0 \times \boldsymbol{d}_e + \epsilon \frac{\partial}{\partial \sigma} \boldsymbol{X}_j^{(2),\epsilon} \times \boldsymbol{d}_e - \epsilon^2 \boldsymbol{t}_0 \times \boldsymbol{d}_e P_{j/i} + O(\epsilon^3) \right], \tag{A 16}$$

where

$$d_e^2 P_{j/i} = (\chi_{j/i}^\epsilon)^2 + 2\chi_{j/i}^\epsilon \boldsymbol{d}_e \cdot \frac{\partial}{\partial \sigma} \boldsymbol{X}_j^{(2),\epsilon} + d_e \left(\frac{\partial}{\partial \sigma} \boldsymbol{X}_j^{(2),\epsilon} \right)^2. \tag{A 17}$$

From the definition of the distance vector $\boldsymbol{X}_i - \boldsymbol{X}_{j/i}$ we know that it has to be normal to the local tangent $\boldsymbol{t}_{j/i}$ at $\boldsymbol{X}_{j/i}$. We use this orthogonality to express the axial displacement $\chi_{j/i}^\epsilon$ in terms of $\boldsymbol{X}_j^{(2),\epsilon}$, $\boldsymbol{X}_i^{(2),\epsilon}$. Thus we require that

$$(\boldsymbol{X}_i - \boldsymbol{X}_{j/i}) \cdot \boldsymbol{t}_{j/i} = 0, \tag{A 18}$$

and use the relations (A 6) and

$$\boldsymbol{t}_{j/i} = \boldsymbol{t}_0 + \epsilon \frac{\partial}{\partial \sigma} \boldsymbol{X}_j^{(2),\epsilon} + o(\epsilon^2), \tag{A 19}$$

to find

$$\chi_{j/i}^\epsilon = -\boldsymbol{d}_e \cdot \frac{\partial}{\partial \sigma} \boldsymbol{X}_j^{(2),\epsilon}. \tag{A 20}$$

With (A 20) the expression $P_{j/i}$ in (A 17) becomes the quadratic form

$$P_{j/i} = \frac{\partial}{\partial \sigma} \boldsymbol{X}_j^{(2),\epsilon} \cdot [\mathbf{1} - \hat{\boldsymbol{d}} \circ \hat{\boldsymbol{d}}] \cdot \frac{\partial}{\partial \sigma} \boldsymbol{X}_j^{(2),\epsilon}, \tag{A 21}$$

where
$$\hat{\boldsymbol{d}} = \frac{1}{|\boldsymbol{d}_e|}\boldsymbol{d}_e, \tag{A 22}$$

and 'o' denotes the tensorial product. The final result for the circumferential unit vector $\boldsymbol{\theta}_{j/i}$ reads, except for errors $o(\epsilon^2)$:

$$\boldsymbol{\theta}_{j/i} = \frac{1}{d_\epsilon}\left(\boldsymbol{t}_0 \times \boldsymbol{d}_e + \epsilon \frac{\partial}{\partial\sigma}\boldsymbol{X}_j^{(2),\epsilon} \times \boldsymbol{d}_e - \epsilon^2 \boldsymbol{t}_0 \times \boldsymbol{d}_e \tfrac{1}{2}[1 - \hat{\boldsymbol{d}} \circ \hat{\boldsymbol{d}}] : \left[\frac{\partial}{\partial\sigma}\boldsymbol{X}_j^{(2),\epsilon} \circ \frac{\partial}{\partial\sigma}\boldsymbol{X}_j^{(2),\epsilon}\right]\right). \tag{A 23}$$

The binormal term $(\Gamma_j/4\pi)(\kappa\boldsymbol{b})_{j/i}\ln(1/r_{j/i})$

Knowing that
$$\kappa\boldsymbol{b} = \boldsymbol{t} \times \kappa\boldsymbol{n} = \boldsymbol{t} \times \boldsymbol{t}_{\tilde{s}}, \tag{A 24}$$

where $\tilde{s}$ denotes an arclength coordinate, and using

$$\boldsymbol{t}_{\tilde{s}} = \frac{1}{|\boldsymbol{X}_s|}\left(\frac{1}{|\boldsymbol{X}_s|}\boldsymbol{X}_s\right)_s = \frac{1}{|\boldsymbol{X}_s|^2}(1 - \boldsymbol{t} \circ \boldsymbol{t}) \cdot \boldsymbol{X}_{ss}, \tag{A 25}$$

$$\boldsymbol{X}_{ss} = \boldsymbol{X}_{\sigma\sigma}^{(2),\epsilon}, \tag{A 26}$$

we find
$$\boldsymbol{t} \times \boldsymbol{t}_{\tilde{s}} = \boldsymbol{t}_0 + \boldsymbol{X}_{\sigma\sigma}^{(2),\epsilon} + O(\epsilon), \tag{A 27}$$

$$\frac{\Gamma_j}{4\pi}\ln\frac{1}{r_{j/i}}(\kappa\boldsymbol{b})_{j/i} = \frac{\Gamma_j}{4\pi}\boldsymbol{t}_0 \times \frac{\partial^2}{\partial\sigma^2}\boldsymbol{X}_j^{(2),\epsilon}\left[\ln\frac{1}{\epsilon^2} + \ln\frac{1}{d_e}\right] + o(1), \tag{A 28}$$

as $\epsilon \to 0$.

The sinusoidal contribution $(\kappa\cos\varphi\boldsymbol{\theta})_{j/i}$

Noting that
$$\kappa\cos\varphi = \boldsymbol{e}_r \cdot \kappa\boldsymbol{n} \quad \text{where} \quad \boldsymbol{e}_r = \frac{1}{|\boldsymbol{d}_e|}\boldsymbol{d}_e = \hat{\boldsymbol{d}}, \tag{A 29}$$

$$\kappa\boldsymbol{n} = \boldsymbol{X}_{\sigma\sigma}^{(2),\epsilon} + o(1) \quad \text{as} \quad \epsilon \to 0, \tag{A 30}$$

we find
$$\frac{\Gamma_j}{4\pi}(\kappa\cos\varphi\boldsymbol{\theta})_{j/i} = \frac{\Gamma_j}{4\pi}\left(\hat{\boldsymbol{d}} \cdot \frac{\partial^2}{\partial\sigma^2}\boldsymbol{X}_j^{(2),\epsilon}\right)\boldsymbol{t}_0 \times \boldsymbol{d}_e + o(1). \tag{A 31}$$

We collect the results from (A 1), (A 2), (A 11), (A 23), (A 28) and (A 31) and we notice that $\boldsymbol{Q}_{j/i}^f$ is the finite part of the Biot-Savart integral for $\mathscr{L}_j$, for which we have presented an explicit asymptotic formula in §2, equations (2.6)–(2.8):

$$\begin{aligned}\frac{\partial}{\partial t}\boldsymbol{X}_i = \frac{\Gamma_i}{4\pi}\Bigg\{&\left(\ln\frac{1}{\delta} + C_i\right)(\kappa\boldsymbol{b})_i + \mathscr{J}[\boldsymbol{X}_i^{(2)}] \times \boldsymbol{t}_0\Bigg\} \\ &+ \sum_{j \neq i}\frac{\Gamma_j}{4\pi}\Bigg\{\ln\left(\frac{1}{\epsilon^2 d_e}\right)(\kappa\boldsymbol{b})_{j/i} + \mathscr{J}[\boldsymbol{X}_j^{(2)}] \times \boldsymbol{t}_0 \\ &+ \left(\frac{1}{\epsilon^2} - \tfrac{1}{2}\boldsymbol{X}_{j,\sigma}^{(2),\epsilon} \cdot [1 - 2\hat{\boldsymbol{d}} \circ \hat{\boldsymbol{d}}] \cdot \boldsymbol{X}_{j,\sigma}^{(2),\epsilon}\right)\frac{2}{d_\epsilon^2}\boldsymbol{t}_{j,e} \times \boldsymbol{d}_e\Bigg\},\end{aligned} \tag{A 32}$$

where $\boldsymbol{t}_{j,e} = \boldsymbol{t}_0 + \epsilon\,\partial\boldsymbol{X}_j^{(2),\epsilon}/\partial\sigma$. The first curly bracket denotes the self-action of the ith vortex, while the sum indicates all the effects of foreign induction. Obviously, the leading contribution to self-induction is the binormal term involving the logarithm $\ln(1/\delta)$, while the dominant foreign-induced velocity is given to leading order by

$$\frac{1}{\epsilon^2}\frac{\Gamma_j}{2\pi d_e^2}\boldsymbol{t}_{j,e} \times \boldsymbol{d}_e = \frac{1}{\epsilon^2}\frac{\Gamma_j}{2\pi}\boldsymbol{t}_0 \times \frac{\boldsymbol{X}_i^{(2)} - \boldsymbol{X}_j^{(2)}}{|\boldsymbol{X}_i^{(2)} - \boldsymbol{X}_j^{(2)}|^2}. \tag{A 33}$$

If we neglect all but these two leading contributions and introduce the distinguished limit

$$\epsilon^2 = \frac{1}{\ln 1/\delta} \tag{A 34}$$

from (2.12), then we obtain a curvature–potential vortex interaction system (1.2) that has been at the core of this paper.

REFERENCES

ABLOWITZ, M. & SEGUR, H. 1981 Solitons and the inverse scattering transform. *SIAM Stud. Appl. Maths* **4**.

ANDERSON, C. & GREENGARD, C. 1989 The vortex ring merger problem at infinite Reynolds number. *Commun. Pure Appl. Maths* **42**, 1123.

AREF, H. 1983 Integrable, chaotic and turbulent vortex motion in two-dimensional flows. *Ann. Rev. Fluid Mech.* **15**, 345–389.

ARMS, R. J. & HAMA, F. R. 1965 Localized-induction concept on a curved vortex and motion of an elliptic vortex ring. *Phys. Fluids* **8**, 553–559.

ARNOLD, V. I. 1989 *Mathematical Methods of Classical Mechanics*, 2nd edn. Springer.

BATCHELOR, G. K. 1967 *An Introduction to Fluid Dynamics*. Cambridge University Press.

CALLEGARI, A. J. & TING, L. 1978 Motion of a curved vortex filament with decaying vortical core and axial velocity. *SIAM J. Appl. Maths* **35**, 148–175.

CHORIN, A. J. 1982 Evolution of a turbulent vortex. *Commun. Math. Phys.* **83**, 517.

CHORIN, A. J. 1988 Spectrum, dimension and polymer analogies in fluid turbulence. *Phys. Rev. Lett.* **60**, 1947–1949.

CHORIN, A. J. 1994 *Vorticity and Turbulence*. Springer.

CHORIN, A. J. & AKAO, J. 1991 Vortex equilibria in turbulence theory and quantum analogues. *Physica* D **52**, 403–414.

CHORIN, A. J. & MARSDEN, J. E. 1990 *A Mathematical Introduction to Fluid Mechanics*. Springer.

CORCOS, G. & LIN, S. 1984 The mixing layer: deterministic models of a turbulent flow. Part 2. The origin of three-dimensional motion. *J. Fluid Mech.* **139**, 67–95.

CROW, S. 1970 Stability theory for a pair of trailing vortices. *AIAA J.* **8**, 2172–2179.

DAMODARAN, K. 1994 Simplified equations for the nonlinear interaction of vortex filaments in 3-D. Undergraduate Senior Thesis supervised by A. Majda, Princeton University.

HASIMOTO, H. 1972 A soliton on a vortex filament. *J. Fluid Mech.* **51**, 477–485.

JIMENEZ, J. 1975 Stability of a pair of co-rotating vortices. *Phys. Fluids* **18**, 1580.

KERR, R. M. & HUSSAIN, A. K. M. F. 1989 Simulation of vortex reconnection. *Physica* D **37**, 474.

KIDA, S. & TAKAOKA, M. 1991 Breakdown of frozen motion fields and vorticity reconnection. *J. Phys. Soc. Japan* **60**, 2184.

KLEIN, R. 1994 Zur Dynamik schlanker Wirbel. Habilitationsschrift, RWTH Aachen, submitted May 2, 1994.

KLEIN, R. & KNIO, O. M. 1995 Asymptotic vorticity structure and numerical simulation of slender vortex filaments. *J. Fluid Mech.* **284**, 275–321.

KLEIN, R. & MAJDA, A. 1991*a* Self-stretching of a perturbed vortex filament I. The asymptotic equations for deviations from a straight line. *Physica* D **49**, 323–352.

KLEIN, R. & MAJDA, A. 1991*b* Self-stretching of perturbed vortex filaments II. Structure of solutions. *Physica* D **53**, 267–294.

KLEIN, R. & MAJDA, A. 1993 An asymptotic theory for the nonlinear instability of anti-parallel pairs of vortex filaments. *Phys. Fluids* A **5**, 369–387.

KLEIN, R., MAJDA, A. J. & MCLAUGHLIN, R. M. 1992 Asymptotic equations for the stretching of vortex filaments in a background flow field. *Phys. Fluids* A **4**, 2271–2281.

LAMB, H. 1932 *Hydrodynamis*, 6th edn. Cambridge University Press.

LOGAN, J. D. 1987 *Applied Mathematics – A Contemporary Approach*. John Wiley & Sons.

MELANDER, M. V. & ZABUSKY, N. 1987 Interaction and Reconnection of Vortex Tubes via Direct Numerical Simulations. *Proceedings IUTAM Symposium on Fundamental Aspects of Vortex Motion*, Tokyo.

MEIRON, D., SHELLEY, M., ASHURST, W. & ORSZAG, S. 1989 Numerical studies of vortex, reconnection. In *Mathematical Aspects of Vortex Dynamics* (ed. R. Caflisch), pp. 183–194. SIAM, Philadelphia, PA.

MOORE, D. W. & SAFFMAN, P. G. 1972 The motion of a vortex filament with axial flow. *Phil. Trans. R. Soc. Lond.* A **272**, 403.

TING, L. & KLEIN, R. 1991 *Viscous Vortical Flows*. Springer.

VAN DYKE, M. 1982 *An Album of Fluid Motion*, Parabolic Press, Stanford, CA.

WIDNALL, S. 1975 The structure and dynamics of vortex filaments. *Ann. Rev. Fluid Mech.* **7**, 141–165.

ZAKHAROV, V. E. 1988 Wave collapse. *Usp. Fiz. Nauk* **155**, 529–533.